Petroleum Science 19 (2022) 882–899

Contents lists available at ScienceDirect

Petroleum Science

journal homepage: www.keaipublishing.com/en/journals/petroleum-science

Review Paper

Application of nanomaterial for enhanced oil recovery

Tuo Liang [a], Ji-Rui Hou [a], Ming Qu [a, *], Jia-Xin Xi [b], Infant Raj [a]

[a] Unconventional Oil and Gas Research Institute, China University of Petroleum, Beijing, PR China
[b] Oil and Gas Technology Research, Changqing Oilfield Branch Company, Xi'an, Shanxi, 710018, PR China

ARTICLE INFO

Article history:
Received 16 June 2021
Accepted 3 September 2021
Available online 13 November 2021

Edited by Xiu-Qiu Peng

Keywords:
Nanoparticle
Preparation method of amphiphilic nanomaterial
Stability
Mechanism
N-EOR

ABSTRACT

Nanofluid offers more opportunities and challenges over the traditional surfactant and polymer solutions during enhanced oil recovery (commonly referred to as tertiary oil recovery) due to its remarkable properties. This review mainly discusses the preparation methods of amphiphilic nanoparticles due to their higher interface activity than sole hydrophilic or hydrophobic nanoparticles (SHNPs). The nanofluids' stability is reviewed in this work. Moreover, the mechanisms of nanofluids in enhancing oil recovery (N-EOR) in terms of interfacial tension reduction, wettability alteration, foam stabilization, emulsion stabilization, structural disjoining pressure, and depressurization-increasing injection are mainly summarized and reviewed. Also, the synergistic effects of nanofluids and traditional surfactants and polymers are discussed. Finally, nanofluids' challenges and prospects are also outlined. The nanofluids can still be regarded as an outstanding candidate for enhancing oil recovery significantly in the future although there are limitations on their applications from laboratory scale to field scale.

1. Introduction

Over recent decades, there has been a distinct contradiction that the amount of produced oil cannot meet the social development needs. Even though renewable energy has grabbed the global market's attention, the demand for crude oil still exists (Aftab et al., 2017; Rezk and Allam, 2019). Hence, crude oil will act as a primary energy source for the development of human society. However, the current methods for recovering oil have been facing severe challenges. Thereby, developing novel technologies or materials for extracting crude oil significantly in the future is essential.

Generally, the crude oil extraction process can be categorized into primary, secondary, and tertiary oil recovery stages. Usually, 40–50% of crude oil can be recovered through the primary (natural energy-driven) and secondary (water-driven) stages, respectively (Ahmed, 2010). After those two stages, tertiary oil recovery techniques are crucial to further extract residual crude oil trapped within reservoir pores and channels. Traditional tertiary oil recovery technologies can be classified into chemical flooding methods, thermal recovery methods, and miscible flooding methods. Miscible flooding refers to the technique that the displacing phase (such as CO_2, flue gas, liquefied petroleum gas, methane, etc.) can mix up with crude oil above the minimum miscibility pressure (MMP) to enhance oil recovery (EOR) due to the disappearance of interfaces. However, miscible flooding also has certain limitations. For example, it is difficult to achieve the required pressure from 610 to 1524 m (Alnarabiji and Husein, 2020). Another obstacle is the formation of gas channeling during the high viscosity oil displacement process. The thermal recovery methods such as steam flooding, huff and puff, and fire reservoir technologies utilize the high temperature to decrease highly viscous oil viscosity. The realistic challenges for widely applying thermal methods are the lower thermal efficiency and higher construction costs (Shah et al., 2010). In terms of chemical flooding processes, injection of surfactant or polymer or alkali solutions into the reservoir helps to reduce the interfacial tension (IFT) of the oil-water interface, alter the wettability of rock (oil-wet to water-wet or neutral-wet) and improve the micro or macro sweep efficiency (Tod et al., 2020; Esfandyari et al., 2020; Klemm et al., 2018; Seetharaman et al., 2020; Shaker Shiran and Skauge, 2013; Tackie-Otoo and Ayoub Mohammed, 2020). However, the degradation of polymers and adsorption of surfactants during the migration forward at harsh reservoir conditions (high temperature, high pressure, and high salinity) limit the usage of chemical agents. Also, chemical agents are not environmentally friendly and economical as the oil price is depressed (Abidin et al., 2012; Negin et al., 2017; Shah et al., 2010).

* Corresponding author.
E-mail address: m.qu@foxmail.com (M. Qu).

https://doi.org/10.1016/j.petsci.2021.11.011

Hence, there is an urgent for new EOR technologies or novel materials to substitute the traditional EOR technologies or agents for enhancing oil recovery.

Nanotechnology has been widely implemented in various sectors like medical, food, electronics, oil, and gas (Konefal et al., 2020; Lee et al., 2018; Li et al., 2017b; Morozovska et al., 2020; Singh et al., 2021; Xiong et al., 2020). Nanotechnologies are commonly referred to as the applications of nanomaterials possessing nano-scale size (1–100 nm) at least in one dimension. Nanomaterials have distinctive properties such as nano-scale size, quantum effects, and massive surface area (AfzaliTabar et al., 2017; Kazemzadeh et al., 2018; Lau et al., 2017). According to their shapes, nanomaterials can be classified into spherical-like shape, rod-like shape, and sheet-like shape (Hong et al., 2006; Qu et al., 2020; Raj et al., 2019; Yan et al., 2013). Over the decades, nanomaterials enhancing oil recovery (N-EOR) technologies have shown significant successes in overcoming the limitations faced by traditional enhancing oil recovery technologies (Foroozesh and Kumar 2020). Nanomaterials are commonly dispersed into specific fluids such as water, ethanol, or other dispersants (forming nanofluids) for improving oil recovery during N-EOR processes. The improvement in oil recovery is due to the massive surface area and dangling bonds of nanomaterials, making them easier to interact with the surrounding materials (AfzaliTabar et al., 2017; Kazemzadeh et al., 2018; Lau et al., 2017; Sofla et al., 2018).

Applications of various nanomaterials for N-EOR have gained considerable attention worldwide. Reported nanomaterials for N-EOR include SiO_2 (Lu et al., 2017), TiO_2 (Sohel et al., 2008), MoS_2 (Qu et al. 2020, 2021), Al_2O_3 (Rezvani et al., 2020), CuO (Bahraminejad et al., 2019), ZnO (Alnarabiji et al., 2018) and graphene (AfzaliTabar et al., 2017). The nanofluids, injected into the oil-bearing area, can reduce IFT of the oil-water interface (Esmaeilzadeh et al., 2014), change the rock surface's wettability from oil-wet to water-wet (Hill et al., 2020), generate structural disjoining pressure at the three-phase contact region (Liang et al., 2020b; Zhang et al., 2016) and reduce oil viscosity (Patel et al., 2018). Although nanomaterials' dosage concentration is lesser than conventional surfactants or polymers, they promise to enhance oil recovery significantly in the future. The prerequisite for broad applications of nanofluids is to guarantee their stability before they are injected into core samples or actual reservoirs with harsh conditions. Unstable nanofluids can reduce reservoir permeability and damage pore-throat structures due to nanomaterials' aggregation and sedimentation behaviors at harsh reservoir conditions (Chakraborty and Panigrahi, 2020). The addition of surfactants or polymers into nanofluids has been conducive to improving nanofluids' stability (Rezk and Allam, 2019; ShamsiJazeyi et al., 2014). Stable nanofluids can migrate deep into the reservoirs and play a significant role in extracting crude oil trapped within reservoir pores and channels.

So far, many articles have reviewed the applications of nanomaterials to improve oil recovery due to their promising prospects (Ali et al., 2020; Hajiabadi et al., 2020; Khalil et al., 2017; Li et al., 2021). Yakasai et al. (2021) has mainly reviewed the effects of various nanomaterial parameters (size, morphology, concentration, temperature, pH value, salinity, etc.) on enhancing oil recovery during flooding processes. Besides, the applications of nanomaterials have also been comprehensively discussed in the IFT reduction, wettability alteration, asphaltene precipitation, and emulsion stability. The manufacturing of bionanomaterials for enhancing oil recovery has been reviewed and discussed by Agi (Agi et al., 2021). However, the large-scale production of bionanomaterials is the major hindrance faced by these materials. Carbon-based nanomaterials have also gained more considerable attention due to their unexpected properties and efficiencies (Sikiru et al., 2021). Hajiabadi et al. (2020) has shown a comprehensive review of the carbon-based nanomaterials on EOR, drilling, formation evaluation and seismic characterization. In addition to study nanofluids for enhancing oil recovery by using physical simulation experiments, the numerical simulation methods are also conducive to facilitating the development of nanofluids in improving oil recovery. Aliu et al. (2020) has reviewed the latest achievements of Lattice Boltzmann methods on studying nanofluids in heat and mass transfer applications. Some other reviews have also discussed the applications of various nanomaterials in EOR, drilling, fracturing and reservoir sensing, etc (Ko and Huh, 2019; Rattanaudom et al., 2021; Zhou et al., 2020). However, there are not many reviews focusing on the synthesis of amphiphilic nanomaterials for the N-EOR. Amphiphilic nanomaterials with hydrophilic and lipophilic nature have more significant advantages in enhancing oil recovery compared to sole hydrophilic or lipophilic nanomaterials (SHNPs). Inspired by this philosophy, this review mainly discusses the preparation methods of amphiphilic nanomaterials. Besides, techniques for evaluating nanofluids' stability and mechanisms about N-EOR (IFT reduction, wettability alteration, foam stability improvement, structural disjoining pressure, etc.) have been also reviewed. We also present both our perspectives and achievements on N-EOR in this work. Moreover, the synergistic effects between nanofluids and chemical agents are also addressed. Finally, the further prospects and challenges faced by nanofluids for further improving oil recovery are also discussed.

2. Synthesis of amphiphilic nanomaterials

Owing to the fascinating and promising properties such as small size effects, quantum size effects and surface effects, nanomaterials have been proved to be excellent materials for EOR. Compared to SHNPs, amphiphilic nanomaterials with hydrophilic and hydrophobic nature have gained more attention across the fields of particulate surfactants, environmental protection, food safety, and energy. That is due to their distinct physicochemical properties like stronger interfacial activity (Aveyard et al., 2003; Lattuada and Hatton, 2011; Lv et al., 2018; Walther et al., 2008; Wan et al. 2017, 2018). In the view of amphiphilic nanomaterials synthesis, plenty of methods have been proposed over the recent decades, including the template masking method (Liu et al., 2013; Wu et al., 2015; Zhang et al., 2013), utilization of specific surface functional groups (Ji et al., 2014) and selective modification via manipulation of π-π stacking interactions (Yang et al., 2016). Generally, the preparation methods of amphiphilic nanomaterials can be categorized into two ways, namely direct preparation and indirect preparation, as shown in Table 1.

Pickering emulsion is one of the most commonly used indirect preparation approaches. It plays a vital role in controlling the shape and morphology of nanomaterials. De Folter et al. (2014) reported Pickering emulsions with cubic and peanut-shaped particles achieved 90% surface coverage, higher than that achieved with ordinary spherical particles. Gao et al. (2014) numerically studied the surface activity of different shapes of amphiphilic nanomaterials and found sphere and rod shapes have only one equilibrium state, but the discotic shape has another metastable state: reverse orientation. The SHNPs of SiO_2 nanoparticles were modified using organic hydrophobic chains through a Pickering emulsion method (Wu et al., 2015). Wu et al. (2020) has also prepared amphiphilic silica nanoparticles using a Pickering emulsion method. Briefly, the SiO_2 nanoparticles were mixed with paraffin wax and water phase to form a Pickering emulsion via stirring. Then, KH550 silane-coupling agent was grafted onto the exposed surface of SiO_2 nanoparticles adsorbed onto Pickering emulsions. After that, lauric acid was added to react with the amino group via the amidation reaction. Finally, the amphiphilic SiO_2–C_{12} nanoparticles were

Table 1
Summary of amphiphilic nanomaterials preparation.

Source	Type	Method	Shape	Size	Simple procedure
Zhang et al. (2013)	Nonsymmetrically amphiphilic graphene	Indirect method (Template masking method)	nanosheet	Less than 100 nm in lateral size, 1.6 nm in the height	①Functionalize the single side of graphene using halogen molecules (Cl, F); ②Coat the poly(methyl methacrylate) (PMMA) film onto the functionalized side; ③Modify another side of graphene using aryl or oxygen-functional groups with the protection of PMMA film;
Wu et al. (2015)	Amphiphilic oxide graphene	Indirect method (Pickering emulsion method)	nanosheet	100–1000 nm in the lateral size, 0.9 nm in the height	①Prepare the wax-in-water Pickering emulsions stabilized by GO; ②Coat the dodecylamine or Poly(propylene glycol) bis(2-aminopropyl ether) molecules onto the exposed side of GO;
Liu et al. (2013)	Amphiphilic Laponite	Indirect method (Surface immobilization method)	Disk	165 nm in the lateral size; 2.8 nm in the height	①Prepare polystyrene (PS) emulsions; ②Stir the mixture after the addition of laponite power into PS emulsions; ③Mix the above mixture and polymerization 2-(Dimethylamino)ethyl methacrylate (PDMAEMA); ④Obtain amphiphilic laponite disks with PS on one side and PDMAEMA on the other side;
Ma et al. (2010)	Amphiphilic silica	Direct method (Utilization of specific surface functional groups)	spherical	20 nm	①Adjust the water solution conditions after silica particles addition; ②Mix silica nanoparticles and cationic surfactants;
Jang et al. (2018)	Amphiphilic silica	Direct method (Manipulating hydrogen bonding method)	spherical	20 nm	①GPTMS hydrolyzes; ②Hydrolysable group connects with the free –OH groups at the surface of the silica nanoparticles;
Liu et al. (2020)	Amphiphilic silica	Direct method (Utilization of specific surface functional groups)	spherical	10 nm	①Mix the NaOH solution and surface-modified silica nanoparticles with Silane coupling agent hexadecyltrimethoxysilane (HDTMS);
Yoon et al. (2012)	Amphiphilic superparamagnetic iron oxide	Indirect method (Pickering emulsion method)	spherical	100 nm	①Synthesize block and random copolymers of poly(acrylic acid) (PAA) and poly(butyl acrylate) (PBA) with hydrophilic and hydrophobic nature; ②Preparation of amphiphilic iron oxide nanoparticles by carboxylate groups of the PAA coordinating with the iron;
Raj et al. (2019)	Amphiphilic MoS_2	Direct method (Utilization of specific surface functional groups)	nanosheet	100 nm in the lateral size; 1.2 nm in the height	①Synthesize pure MoS_2 nanosheets; ②Mix pure MoS_2 nanosheets and octa decyl amine (ODA);
Luo et al. (2018)	Amphiphilic graphene oxide	Direct method (Manipulating hydrogen bonding method)	nanosheet	around 250 nm in the lateral size	①Mix GO and tapioca microspheres; ②Graft the alkylamine molecules onto the exposed GO surface;
Qu et al. (2021)	Amphiphilic MoS_2	Direct method (Utilization of specific surface functional groups)	nanosheet	75 nm in the lateral size; 1.2 nm in the height	①Synthesize pure MoS_2 nanosheets; ②Mix pure MoS_2 nanosheets and rhamnolipid molecules;
Yang et al. (2016)	Amphiphilic graphene oxide	Indirect method (Electrostatic assembly method)	nanosheet	500 nm in the lateral size; 39 nm in the height	①Synthesize graphene oxide (GO) nanosheets; ②Mix polystyrene chains with GO nanosheets (PS-GO microspheres); ③Mix poly(2-(dimethylamino)ethyl methacrylate (PDMAEMA) with PS-GO microspheres;

obtained after centrifugation. Besides, amphiphilic graphene oxide nanosheets can be prepared using a template polymer or be defunctionalized by altering the ionic strength based on electrostatic assembly. Yang et al. (2016) had successfully prepared amphiphilic graphene oxide nanosheets possessing hydrophobic polystyrene chains on one side and hydrophilic poly(2-(dimethylamino)ethyl methacrylate) chains on the other side. This method is first to protect one side of nanoparticles and then functionalize another side. Although this method is popular because of its mild and straightforward, the graft effect depends on the preparation of individual nanoparticle, which is difficult to control.

There are two ways for direct preparation based on the sol-gel method: emulsion interface self-assembled sol-gel and template-assisted sol-gel. Silica amphiphilic nanosheets were prepared by crushing Janus hollow spheres synthesized at the self-assembled materialization of an amphiphilic emulsion interface (Liang et al., 2011). The synthesized Janus nanosheets, as particulate surfactants, can be used to reduce oil-water interfacial tension and then collect oil drops. The flexible amphiphilic nanosheets (3-butyldianhydride mercaptopropyltrimethoxysilane (BDMPS)) can be prepared through a self-assembled monolayer of an amphiphilic silane on a template (Liu et al., 2015). They are used as solid emulsifiers. The template-assisted sol-gel method can be used to prepare smaller thickness amphiphilic nanosheets over the emulsion interface self-assembled sol-gel approach. Graphene oxide (GO)-based amphiphilic nanosheets have been synthesized via manipulation of hydrogen bonding. The GO and tapioca starch microspheres were evenly dispersed in the water phase. Then, GO

was adsorbed onto the surface of tapioca starch microspheres via hydrogen bonds. Finally, the single-side surface hydrophilization of GO transformed into a hydrophobization surface by functionalizing alkylamine molecules, as shown in Fig. 1. The amphiphilic nanosheets were released from the starch microspheres by sonication and heating in ethanol (Luo et al., 2018). Another direct approach for preparing amphiphilic nanomaterials is the hydrothermal reaction process. The SHNPs of MoS_2 nanosheets were synthesized through a simple hydrothermal method firstly, and then the surfaces of pure MoS_2 nanosheets were functionalized using CTAB or ODA molecules (Qu et al., 2021; Raj et al., 2019).

Amphiphilic nanomaterials can also be classified into spheres, nanosheets, and rods according to their shapes. The interfacial activity of amphiphilic nanosheets is more significant than that of amphiphilic spheres or rods, resulting in more considerable desorption energy from the interface to the bulk phase (Jia et al., 2016; Wei et al., 2018). As a result, amphiphilic nanosheets can be employed to effectively improve emulsion and foam stability once adsorbed onto interfaces, eventually improving oil recovery (Jia et al., 2016).

3. Nanofluid stability

Nanofluid is defined as the dispersion of nanomaterials in a specific dispersant (water, ethanol, etc.) at a particular concentration. It is crucial to evaluate the stability of nanofluids before they are injected into reservoirs. They are thermodynamically unstable. Nanomaterials in the bulk phase tend to aggregate to decrease the system energy due to the high surface energy. Nanofluid stability evaluation can be done using the solid sedimentation method, Zeta potential measurement, and spectral analysis.

3.1. Sedimentation method

The sedimentation method for assessing nanofluid stability is the most intuitive and pervasive technique. This method measures the weight or volume of sediment with time at the bottom of the liquid column. Meanwhile, photographs of the dynamic deposition process can be recorded as an essential indication to determine nanofluids' stability qualitatively, as shown in Fig. 2. Chakraborty et al. (2017, 2018) took sedimentation photographs to evaluate the stability of Cu–Al LDH and TiO_2 nanofluids kept in a glass vial over time. The results showed that the stability of nanofluids was directly related to particle size. The phenomenon of poor stability and faster sedimentation rate of nanofluids is likely to be occurred in a specific fluid due to larger particle size. Besides, copper and Al_2O_3 nanofluids' stability was also determined using the sedimentation method (Li et al., 2007; Zhu et al., 2009). However, this method requires more time to observe nanofluids' change trends and capture high-quality photographs as an intuitive indication.

3.2. Zeta potential measurement

Zeta potential measurement has also been commonly used to determine suspension stability (Chakraborty and Panigrahi, 2020). Electrostatic repulsion exists between adjacent nanoparticles in the nanofluids due to the same charge on nanoparticles' surfaces. This phenomenon positively inhibits particle coalescence and then improves nanofluid stability (Ismay et al., 2013). On the other hand, van der Waals force, widely existing among particles, is an attractive force that is not conducive to nanofluids' stability. The Zeta potential, consisting of electrostatic repulsion force and van der Waals force, is a comprehensive reflection index. The higher value of Zeta potential represents higher repulsive force and better nanofluid stability (Cacua et al., 2019). The Au nanofluids with excellent stability were prepared by Kim (Kim et al., 2009). The outstanding stability of Au nanofluids was ascribed to the larger negative Zeta potential values among Au nanoparticles in the water phase. In general, stable suspensions signify that bulk suspensions' absolute Zeta potential value is greater than 30 mV (Esfandyari et al., 2015; Fatehah et al., 2014). In other words, nanofluids with a lower absolute Zeta potential value tend to agglomerate faster than the nanoparticles with a higher absolute Zeta potential value. Cacua et al. (2019) studied the effects of surfactant concentrations and pH values on Zeta potential values of alumina nanofluids. The results revealed that higher absolute Zeta potential values represent the smaller average diameter of alumina nanoparticles. Also, the higher stability of magnetic graphite nanofluid can be obtained when the Zeta potential was around 41.3 mV (Souza et al., 2012). In general, the Zeta potential value of suspensions can be affected by ionic strength (ion type), pH value, temperature, etc.

Known from DLVO theory, nanoparticles possessing surface charge in the nanofluids can attract opposite charges around them after those nanoparticles are evenly dispersed in a specific fluid.

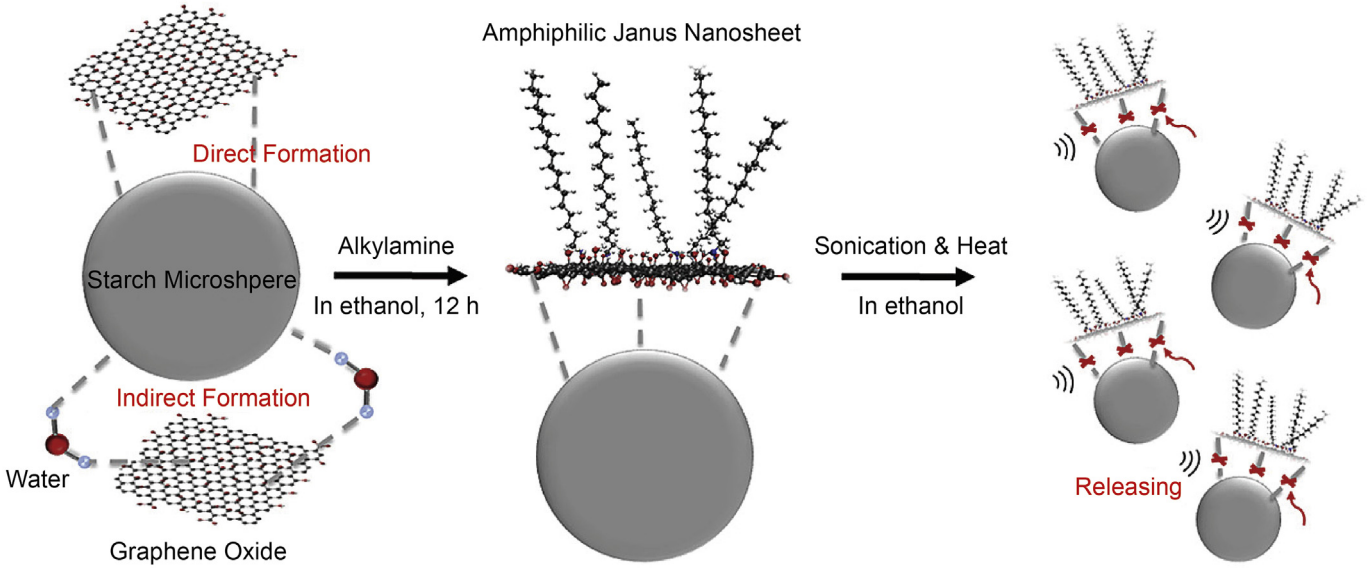

Fig. 1. Synthesis of graphene-based amphiphilic nanosheets via hydrogen bonding (Luo et al., 2018).

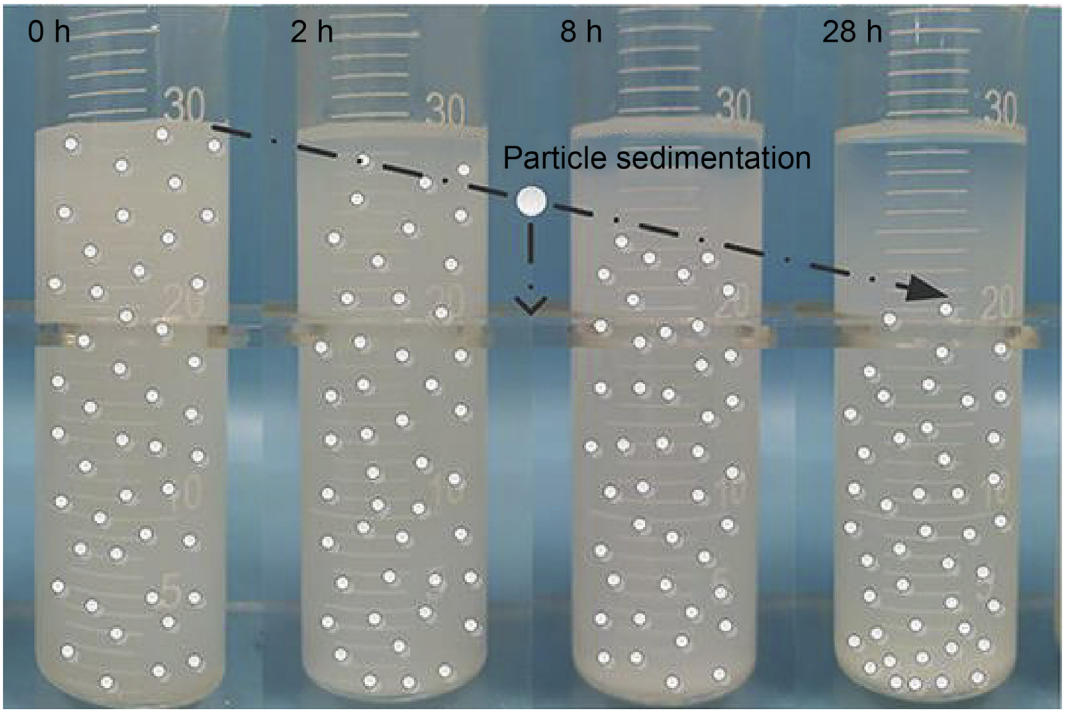

Fig. 2. Time-lapse images of nanofluid destabilizing over time (Sun et al., 2020).

Adsorbed opposite ions can form a diffused electric double-layer, including a dense layer (Stern layer) and a loose layer (Diffuse layer) (Gomez-Flores et al., 2020). For instance, the diffused electric double-layer structure around negatively charged nanoparticles is exhibited in Fig. 3. It can be seen that the oppositely charged ions distribute around the nanoparticle. Zeta potential (repulsion force) formed between diffuse layers (at the slipping plane) effectively prevents nanoparticles from contacting and agglomerating. The thickness of the diffused electric double-layer, referring to as "Debye length", can also limit these nanoparticles' trajectory. Therefore, a stable dispersion can be formed at a higher repulsion force and longer Debye length among nanoparticles (Bukar et al., 2014; French et al., 2009; Lombardo et al., 2015).

The addition of opposite charge ions can compress the thickness of the diffused electric double-layer and reduce the value of Zeta potential at the slipping plane. In other words, the addition of opposite charge ions can lead to an unstable dispersion (Saleh et al., 2008). The effects of different valent ions on both the thickness of the diffused electric double-layer and Zeta potential values are significantly different (Ji, 2014). At the same concentration, the effects of different valent ions on Zeta potential value have the following logical relationship: trivalent > bivalent > monovalent. In addition to ion strength, pH value also has a pronounced effect on nanofluids' stability, which is commonly related to another indicator (isoelectric point). The isoelectric point is defined as the pH value of a dispersion system when the Zeta potential of dispersion is equal to zero. The dispersion is the least stable at the isoelectric point (Keller et al., 2010). Fig. 4 shows the effects of pH value on the nanofluid stability and the isoelectric point for a specific nanofluid. It is essential to evaluate the nanofluids' electrification performance to avoid nanoparticles' adsorption on the rock surface and accumulation among nanoparticles at the harsh reservoir conditions during N-EOR processes.

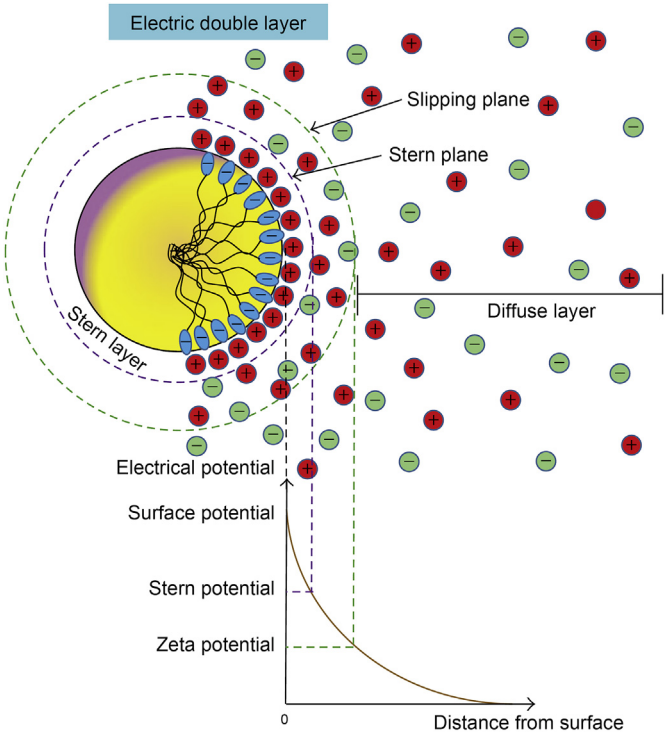

Fig. 3. Schematic representation of diffused electric double-layer around charged nanoparticles (Lombardo et al., 2015).

3.3. Spectral method

Another method to determine nanofluid stability is spectral analysis. Here, we mainly discuss the spectral analysis methods: spectral absorbance analysis method and multiple-light scattering

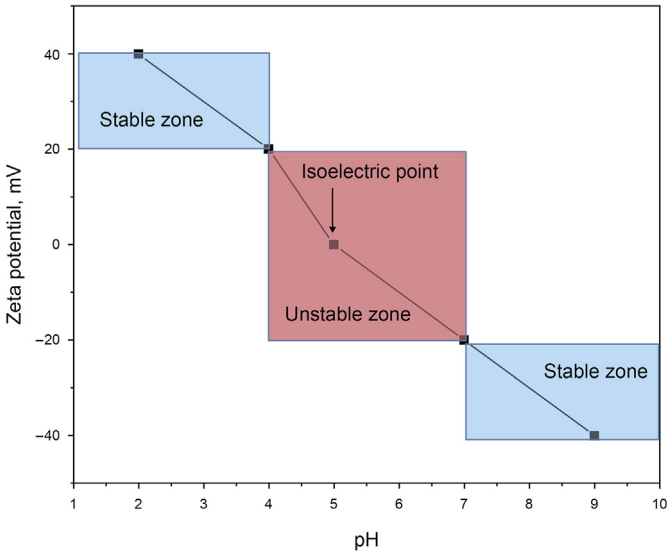

Fig. 4. Effect of pH values on the stability of nanofluids (Pate and Safier, 2016).

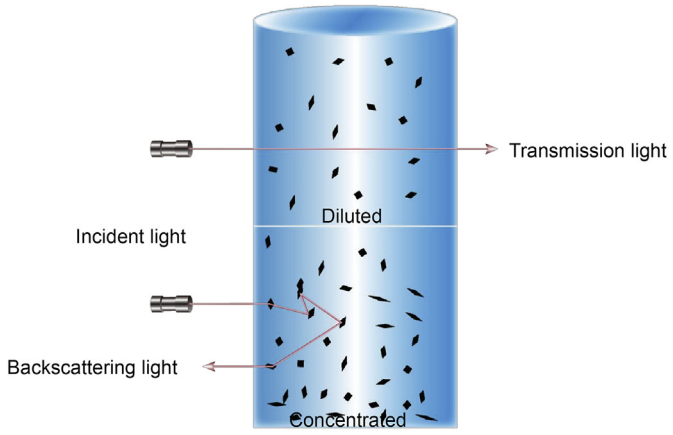

Fig. 5. The principle of TURBISCAN Lab Expert stability analyzer.

method. Based on the Beer–Lambert Law, the spectral absorbance analysis method detects the absorption of incident light with a specific wavelength by nanoparticles using a UV–vis spectrophotometer. The absorbance of nanoparticles can be significantly affected by nanoparticle concentration, and there is a relationship between the absorbance and concentration of nanoparticles (Eq. (1)). Therefore, nanoparticle concentration can be calculated by detecting nanofluid absorbance in the same position over time. Finally, the stability of nanofluids can be determined by nanoparticle concentration over time. For example, the UV–vis spectrophotometer was introduced to investigate the relationships between MWNT concentrations and MWNT nanofluids' stability at different sediment times (Chen and Xie, 2010). The purpose can be achieved by detecting the UV–vis absorbance value at various MWNT concentrations and different sediment times. The alumina and copper nanofluids' stability was also evaluated using a spectrophotometer after the nanofluids were deposited for 24 h (Huang et al., 2009). Besides, the stability of FePt nanofluids was investigated and measured by using spectrophotometer analysis (Farahmandjou et al., 2009).

$$A = \log\frac{I_0}{I} = abc \tag{1}$$

Where A is the absorbance, I_0 represents incident light intensity, I represents transmission light intensity, a represents molar absorption coefficient, b is liquid height, and c is the concentration of nanoparticles.

The Multiple-Light Scattering method detects the intensity change of transmittance light and back-scattering light using the Turbiscan Lab Expert Stabilizer when a pulsed near-infrared light ($\lambda = 880$ nm) source passes through the sample pool. The micro-migration behaviors (agglomeration and sedimentation behaviors) of nanoparticles in the bulk phase can be characterized by analyzing the spectrum changes (transmission light spectrogram or back-scattering light spectrogram) with the time and height of the sample. A detailed analysis of the spectrogram can be found in our previous work (Liang et al., 2020a). The schematic diagram of the multiple-light scattering method is shown in Fig. 5. Apart from spectral analysis, nanofluid's stability can be quantitatively described using *TSI*, short for the Turbiscan Stability Index. The lower the *TSI* value is, the more stable the nanofluid is. Eq. (2) is used to calculate the *TSI* value.

$$TSI = \sum_i \frac{\sum_h |\mathrm{scan}_i(h) - \mathrm{scan}_{i-1}(h)|}{H} \tag{2}$$

Where i is scanning number; h is scanning point height; $\mathrm{scan}_i(h)$ is the average light intensity; H represents the number of sample scanning data points.

Apart from the above three main methods, there are several other ways to evaluate nanofluid stability. According to the Stokes Eq. (3), nanoparticles' settling velocity is proportional to the square of nanoparticle diameter. Hence, nanoparticles with smaller sizes result in more stable dispersion. The diameter distribution of nanoparticles can be measured using a dynamic light scattering (DLS) technique.

$$v = \frac{1}{18}\left[\frac{\Delta\rho g d^2}{\eta}\right] \tag{3}$$

where v is the settling velocity, $\Delta\rho$ represents the density difference of the solid phase (nanoparticles) and dispersed medium (water phase), g is the acceleration of gravity, d is the nanoparticle diameter, and η represents the viscosity of the dispersed medium.

Except for the previously mentioned factors affecting nanofluid stability, nanofluid stability can also be affected by dispersant types, temperature, and surface groups. For instance, nanomaterials' surface modification has been commonly implemented to improve nanofluid stability (Kamiya and Iijima, 2010; ShamsiJazeyi et al., 2014). The surface-modified agents include surfactants, polymers, silane coupling agents, and other organic or inorganic materials. The surface-modified agents coating on the nanomaterial surface can improve repulsion force and steric hindrance among nanoparticles to keep them dispersed well (Kamiya and Iijima, 2010; Li et al., 2020; Wei et al., 2018). The silica nanoparticles were modified using zwitterionic and hydrophilic silanes by Hadia (Hadia et al., 2021). The results found that the coated silica nanoparticles can remain stable for at least 6 months. Extensive discussions on how to improve nanofluid stability can be seen in other reviews focusing on nanofluid stability (Chakraborty and Panigrahi, 2020; Heinz et al., 2017).

4. Mechanisms of nanofluids on N-EOR

4.1. Interfacial tension

Meniscus interface locating at the two immiscible phases contact region is formed due to interfacial tension, resulting in an uneven displacement front and lower oil recovery during flooding. Therefore, it is crucial to improve oil displacement efficiency by reducing the interfacial tension at the microscopic level (Zhao and Wen, 2017). Many studies confirmed that nanomaterials' addition to the displacing fluid can reduce the IFT, which leads to the oil recovery improvement (Hendraningrat and Torsaeter, 2015; Roustaei et al., 2013; Zaid et al., 2013). For instance, γ-Al_2O_3, MgO, and TiO_2 nanoparticles showed great IFT reduction ability (Nowrouzi et al., 2019). The IFT value of the nanofluids-crude oil interface is inversely proportional to the temperature and salinity and directly proportional to the nanoparticle concentration and pressure (Nowrouzi et al., 2019). Nanofluids can decrease IFT of the oil-water interface because of the formation of nano-layers at the oil-water interface. After nanomaterials' adsorption at the oil-water interface, the interfacial properties (interface energy) can be changed. Du et al. (2010) found that the binding energy (ΔE) of nanomaterials at the oil-water interface can be determined by oil-water interfacial tension, according to Eq. (4):

$$\Delta E = -\frac{(\gamma_0 - \gamma)\pi R^2}{\eta} \tag{4}$$

Where γ_0 represents the interfacial tension of the system in the absence of nanomaterials, γ represents the interfacial tension of the system in the presence of nanomaterials, η is the fraction of area occupied by nanomaterials at the oil-water interface, and R is the hydrodynamic radius of nanomaterials.

However, some researchers also demonstrated that SHNPs have no contributions to IFT reduction (Biswal and Singh, 2016; Fereidooni Moghadam and Azizian, 2014; Ma et al., 2008; Pichot et al., 2012). Metin et al. (2012) found that SHNPs (silica nanoparticles) cannot adsorb onto the decane-water interface and did not significantly affect the IFT of the decane-water interface because they are not amphiphiles. Moreover, the results showed that IFT of the decane-water interface in the presence of SHNPs was not sensitive to their particle size and concentration.

Amphiphilic (Janus) nanomaterials were identified to reduce interfacial tension. Amphiphilic nanomaterials can promote the adsorption of amphiphilic nanomaterials onto the oil-water interface, resulting in IFT reduction significantly. Li et al. (2018a) revealed that the adsorption arrangement of amphiphilic nanomaterials (active nanoparticles) and SHNPs were different due to surface functional groups (Fig. 6). SHNPs distribute in one side of the bulk phase at the oil-water interface. This adsorption equilibrium of SHNPs at the oil-water interface can be easily broken under external force. On the contrary, the amphiphilic nanoparticles can adsorb at the oil-water interface and evenly distribute in both the water and oil phases. Those adsorption behaviors significantly reduce interfacial tension and improve interfacial viscoelasticity due to forming a stable and stronger nanometer interfacial film over SHNPs (Qu et al., 2020). Qu et al. (2020) reported that the IFT between simulated oil consisting of kerosene and paraffin and CTAB-MoS_2 nanofluid could be decreased to 14.9 mN/m compared to DI water-simulated oil system (IFT ~ 36 mN/m). Besides, the IFT of the decane-water interface in the presence of silica nanoparticles modified with PEG showed a dramatic decrease trend as nanoparticle concentration increased or nanoparticle diameter decreased (Metin et al., 2012). As a result, the excellent interfacial activity of amphiphilic nanoparticles is beneficial for improving oil recovery during N-EOR by reducing IFT.

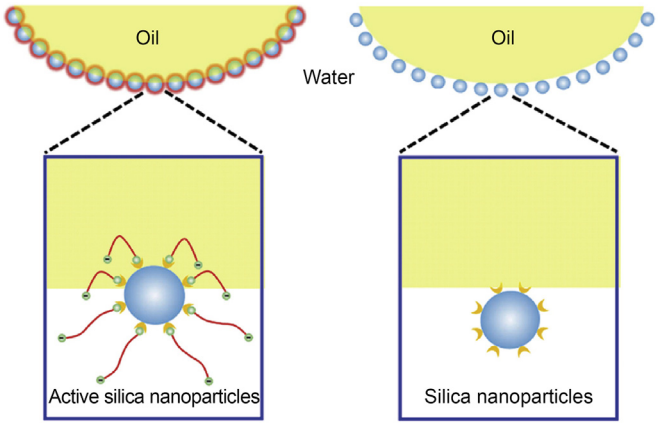

Fig. 6. Schematic illustration of amphiphilic silica nanoparticles (left) and SHNPs (right) at the oil–water interface (Li et al., 2018a).

IFT of the oil-water interface is an indicator that strongly influences oil recovery. Capillary number theory is proposed based on C-EOR technologies, such as surfactant and polymer flooding. It can also be introduced to explain the displacement mechanisms of nanofluids to some extent. Known from capillary number theory (N_c), Eq. (5), IFT reduction results in a decreased capillary force, thereby improving the capillary number. The larger the capillary number is, the more favorable it is for oil displacement.

$$N_c = \frac{viscous\ force}{capillary\ force} = \frac{\mu \times \nu}{\sigma \times \cos\theta} \tag{5}$$

where μ represents dynamic viscosity of displacing fluid, ν is Darcy velocity displacing fluid, σ is interfacial tension between the displaced and displacing fluid, and θ is the contact angle.

However, it should be noted that nanomaterials have many unique properties and interfacial behaviors over traditional surfactants. For instance, surfactants can adsorb at the oil-water interfaces in the form of a single layer according to monolayer adsorption theory (Zhou et al., 2018). After surfactants reach saturated adsorption at the oil-water interface, surfactants preferentially form micelles in the bulk phase. However, nanomaterials can adsorb at the oil-water interface and form multilayer adsorption (Qu et al., 2020; Raj et al., 2019). Compared to surfactant adsorption, nanomaterials' adsorption behaviors may lead to distinct interfacial properties, significantly contributing to oil recovery. Therefore, an urgent need for theory to better understand nanofluid flooding mechanisms during the N-EOR process is necessary.

4.2. Wettability alteration

Most of the reservoir matrix possesses oil-wet (hydrophobic) nature because of the crude oil environment around its surface. Oil-wet rock surface indicates the firm adhesion of crude oil onto the rock surface, leading to an oil film's formation. Thus, more energy is required to exfoliate oil film from the rock surface. Besides, the pressure difference (capillary force) at the curved oil-water interface is pointed into the displacing phase (water phase) due to the oil-wet rock surface. The capillary force is resistant to crude oil's flow, resulting in low oil recovery. Therefore, wettability alteration of rock surface from oil to water-wet or oil to neutral-wet is favorable for enhancing oil recovery. The wettability of the rock

surface can be determined by measuring its contact angle (CTA). The CTA for an oil-wet surface is greater than 105°, while for a neutral-wet surface, CTA ranges from 75° to 105°. When the CTA is lower than 75°, the rock surface denotes water-wet characteristics.

Recently, it is proved that nanoparticles can effectively spread onto the solid surface to change the rock surface's wettability. SiO_2 nanoparticles with super-hydrophilic surfaces were used to decrease contact angle from 100° to 0° on the aged glass (Maghzi et al., 2012). Karimi et al. (2012) proposed that the change of contact angle of carbonate reservoir rock surface treated with zirconium oxide (ZrO_2) nanofluid was ascribed to the formation of nanoparticle structuring (they called "nanotextured surfaces" on the rock surface). According to their theory, nanotextured surfaces' formation changing the wettability of carbonate rock surfaces can take up at least 2 days. Besides, the effects of wettability on oil recovery using polymer-coated silica nanoparticles were comprehensively studied by Omran (Omran et al., 2020). The results revealed that the polymer-coated silica nanoparticles could change the oil-wet glass with a contact angle of 143.30° into a water-wet glass with a contact angle of 48.75°. Some studies suggested that wettability alteration from oil-wet to strongly water-wet showed more fantastic effects on enhancing oil recovery than weakly water-wet. Hadia et al. (2021) evaluated the ability of coated silica nanoparticles to change the solid surface's wettability on aged sandstone and carbonate rock surfaces. The results showed that the coated silica nanoparticles can alter the wettability to water-wet by adsorbing on rock surfaces. Besides, the coated silica nanoparticles can be more effective in changing the wettability of carbonate surface instead of sandstone surface. The synergistic effects of ZrO_2 nanoparticles and different nonionic surfactants on the wettability alteration of carbonate samples were investigated by contact angle measurement (Karimi et al., 2012). Results showed that the strongly oil-wet rock surface could transform into a strongly water-wet surface after treatments using different nanofluids. Moreover, three types of Fe_3O_4 nanoparticles (SHNPs, coated with EDTA, coated with SLS) were systematically studied to change the wettability of a carbonate rock surface substrate from oil-wet to water-wet (Shalbafan et al., 2019). Findings revealed that Fe_3O_4 nanoparticles coated with EDTA/SLS can dramatically decrease the carbonate substrate contact angle of 140° (strongly oil-wet) to 27° and 22° (strongly water-wet), respectively. Furthermore, they also demonstrated that the increase in aging temperature positively affected wettability alteration, while increasing pressure had a negligible effect. The electro-kinetic method was also proposed to study the wettability alteration (Dehghan Monfared and Ghazanfari, 2019). The rock surface wettability can be determined by detecting electro-kinetic parameters change (streaming potential coupling coefficient and Zeta potential) during the wettability alteration processes. The most significant advantage of this method considers the pore-throat structure during wettability alteration processes compared to the contact angle measurement.

The water-wet surface represents that water can adhere to rock surfaces to form a water film. The thickness of water film increases with the increase of water-wet degree (He and Hua, 1998). As a result, the flow channel's diameter for crude oil is also relatively decreased, especially in a low permeability reservoir. The decrease in the flow channel's diameter leads to high injection pressure and low oil recovery. In the case of a neutral wet surface, the piston displacement mode is expected to be achieved. Owing to the reduction of the core sample's hydrophilicity, the improvement of oil recovery efficiency was achieved as functionalized silica nanoparticles were injected into the water-wet core (Roustaei et al., 2013). An investigation of nanofluid with respect to its ion strength on wettability alteration of carbonate surface was performed (Hou et al., 2019). Results showed that the presence of Na^+ can promote the adsorption of nanoparticles on the rock surface by neutralizing the negatively charged portion that existed on the carbonate surface.

4.3. Foam stabilization improvement

Foam flooding is one of the promising techniques, which has been widely used to recover crude oil from reservoirs. The oil recovery efficiency of foam flooding is improved due to the delay of gas channeling, improvement of sweep efficiency (Li et al., 2016), increase of oil displacement efficiency (Li et al., 2019a), and adjustment of mobility ratio (Sun et al., 2015). Yang et al. (2021) reported the synergy of hydrophilic nanoparticles (T40) and nonionic surfactants ($C_{12}E_{23}$) on CO_2 foam stability at elevated temperatures and extreme salinities. Sandpack experimental results indicate that the $C_{12}E_{23}$/T40 foam can enhance the oil recovery 20.1% after water flooding by increasing the sweep area and flooding efficiency. However, foam is generally considered a thermodynamically and kinetically unstable system. Foam can be destroyed by an external force, especially under harsh reservoir conditions (high temperature, high salinity, high crude oil saturation). To overcome those barriers, foam stabilizers such as polymer, solid particles, and gels can be introduced to improve foam stability. The primary mechanism for polymer and gel additions is improving the viscosity of interfacial film, leading to a lower gas flow speed between adjacent bubbles. However, improved viscosity of foam leads to the difficulty of foam injection into the reservoirs. It is observed that the nanoparticles' addition into foam liquids can improve foam stability and foamability by adsorbing onto the gas-liquid (AlYousef et al., 2017). Yin et al. (2018) showed that cellulose and surfactant synergism can significantly improve foam stability by increasing the interfacial film thickness and delaying the liquid drainage. Yang et al. (2017) reported that modified AlOOH nanoparticles can be utilized to stabilize foam generated by SC (Sodium cumene sulfonate) at a broad range of concentrations. Nitrogen and methane foam were also generated using surfactant-nanoparticle-based fluid, and the properties of foam at the presence or absence of nanoparticles were also analyzed systematically (Xu et al., 2020). Results showed that the based fluid viscosity and foam stability were significantly improved after the addition of 1.0 wt% SiO_2. Besides, more than 30% of oil recovery factors can be enhanced using surfactant-NP foam flooding over surfactant foam flooding. Fig. 7 shows the mobilizing oil mechanisms when foam contacts with residual oil during foam migration forward at the presence or absence of nanoparticles. The shape of surfactant foam tends to deform under the action of external force. Meanwhile, foam is inclined towards the flow over the residual oil drop, as shown in Fig. 7b. Compared with surfactant foam, surfactant-NP foam exhibits an excellent ability to keep its spherical structure while contacting with residual oil drop, as shown in Fig. 7d. The dense arrangement of nanoparticles at the liquid-gas surfaces strongly increases the film thickness and strength, which can inhibit foam deformation and then generate a stable foam. Consequently, an additional force at the contact region of surfactant-NP foam and oil drop is generated to effectively mobilize residual oil drop trapped within reservoir pores and throats.

The type of used surfactants, concentration, the size distribution of nanoparticles, and type of nanoparticles (contact angle) can affect the stability of the surfactant-NP foam. Here, desorption energy theory is mainly employed to interpret the mechanisms of foam stabilized by nanoparticles.

4.3.1. Desorption energy of a single spherical nanoparticle

A single spherical nanoparticle is considered to be adsorbed onto the gas-water interface, as shown in Fig. 8a. The following Eqs

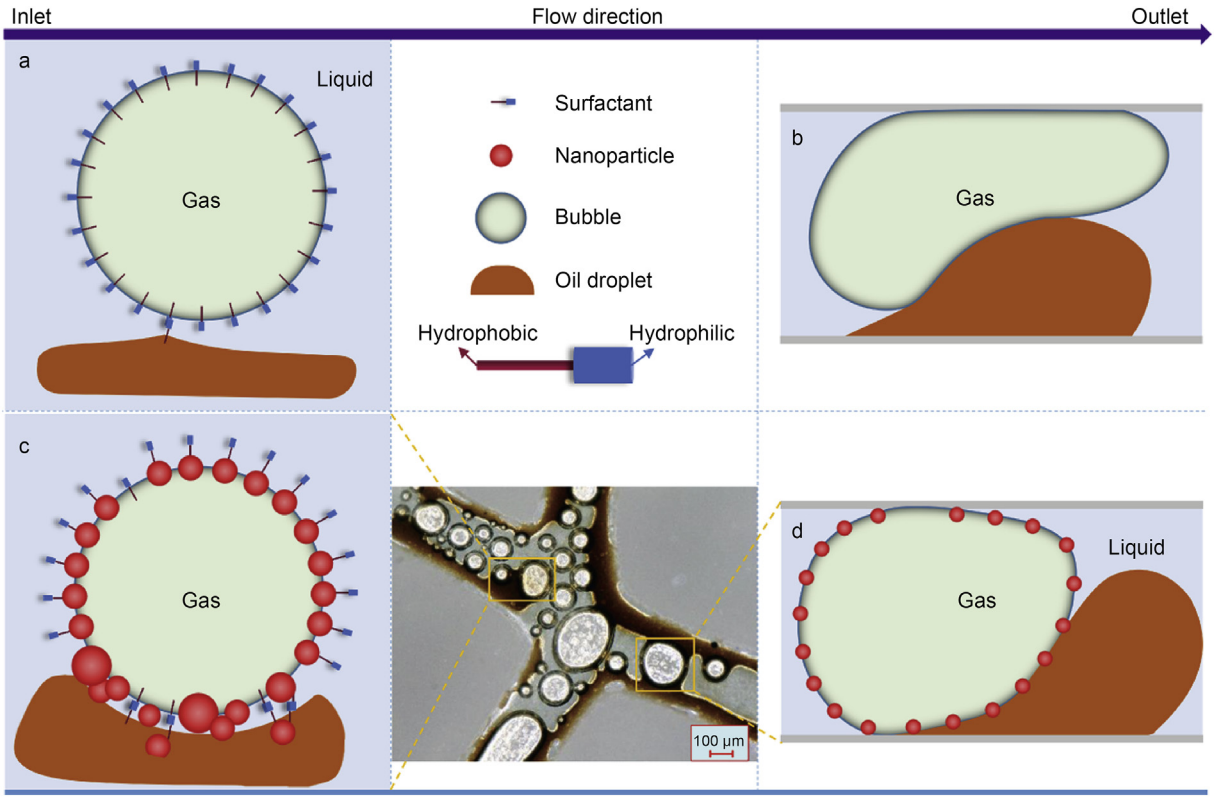

Fig. 7. Schematic of foam at the presence or absence of nanoparticles during mobilizing residual oil drop process, **(a) and (c)** differences in crude oil adsorption of the surfactant foam and the surfactant-NP foam, **(b) and (d)** differences in the degree of deformation of the liquid film for the surfactant foam and surfactant-NP foam (Xu et al., 2020).

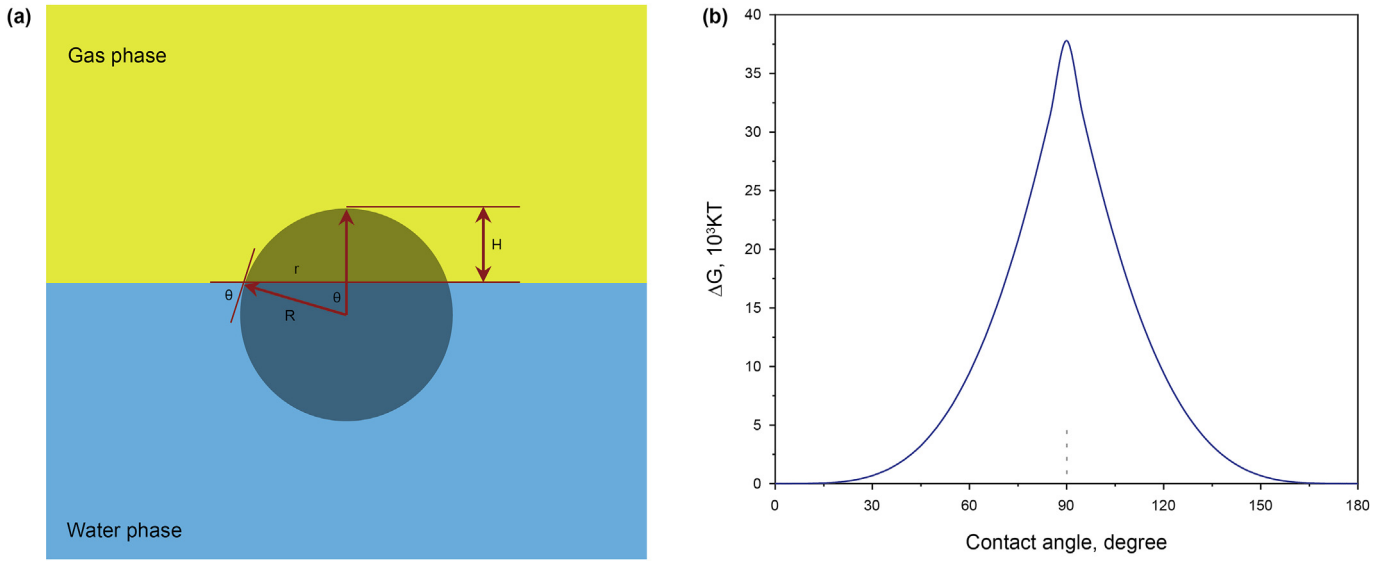

Fig. 8. **a** A single spherical nanoparticle adsorbed at the gas-water surface, **b** desorption energy of a specific nanoparticle (*R*, 30 nm).

for desorption energy of spherical particles come from the previously published paper (Binks and Lumsdon, 2000). Eq. (6) shows the contributed surface energy of the gas phase.

$$\Delta E_{sg} = A_{sg} \times \gamma_{sg} \tag{6}$$

Area immersed in the gas phase is calculated according to Eq. (7) given below:

$$A_{sg} = \int_0^{\theta} 2\pi r \times R d\theta = \int_0^{\theta} 2\pi R^2 \sin\theta d\theta = 2\pi R^2 (1 - \cos\theta) \tag{7}$$

Hence, the ΔE_{sg} can be obtained from Eq. (8):

$$\Delta E_{sg} = 2\pi R^2 (1 - \cos\theta)\gamma_{sg} \tag{8}$$

Similarly, the surface energy contributed by the water phase is calculated from Eq. (9):

$$\Delta E_{sw} = 2\pi R^2(1+\cos\theta)\gamma_{sw} \tag{9}$$

The surface energy contributed by the eliminated gas-water interface owing to the presence of spherical nanoparticle is calculated, Eq. (10):

$$\Delta E_{gw} = \pi r^2 \gamma_{gw} = \pi R^2 \sin\theta^2 \gamma_{gw} = \pi R^2\left(1-\cos\theta^2\right)\gamma_{gw} \tag{10}$$

As a result, the required energy to remove the single adsorbed spherical nanoparticle to the water phase can be determined according to Eq. (11):

$$\Delta G = 2\pi R^2(1-\cos\theta)\left(\gamma_{sw}-\gamma_{sg}\right) + \pi R^2\left(1-\cos\theta^2\right)\gamma_{gw} \tag{11}$$

Known from the Young Eq. (12):

$$\gamma_{sg} - \gamma_{sw} = \gamma_{gw}\cos\theta \tag{12}$$

Eq. (11) can be simplified to Eq. (13):

$$\Delta G = \pi R^2 \gamma_{gw}(1-\cos\theta)^2 \tag{13}$$

Similarly, the required energy to remove the single adsorbed nanoparticle to the gas phase can be determined according to Eq. (14):

$$\Delta G = \pi R^2 \gamma_{gw}(1+\cos\theta)^2 \tag{14}$$

According to Eqs. (13) and (14), the desorption energy of s single spherical nanoparticle from the surface to the bulk phase is calculated and drawn in Fig. 8b as a function of the contact angle of the nanoparticle surface. Several parameters of nanoparticle radius (R, 30 nm), surface tension (γ_{gw}, 55 mN/m), and temperature (298 K) are given to calculate a single spherical nanoparticle's desorption energy. It can be concluded that when the contact angle is 90° the maximum desorption energy is achieved. This denotes that the nanoparticles are not easily desorbed from the surface to the bulk phase. From Fig. 8b, it is observed that a single nanoparticle needs about dozens of thousand K_BT to desorb from the surface to the bulk phase. Compared to surfactant needing several K_BT, nanoparticles show a significantly potential ability to stabilize foam.

4.3.2. Desorption energy of a single nanosheet

As mentioned above, nanosheets can also be used to stabilize foam as a stabilizer. Similar to the desorption energy theory of a single spherical nanoparticle, we propose a new desorption energy Eq for single nanosheet desorption from the surface to the bulk phase. The assumptions used to derive the Eq are given below:

1 The thickness is negligible relative to its length and width;
② The nanosheet adsorbed at the surface is completely spread out. The adsorption schematic of a single nanosheet is shown in Fig. 9a.

The unilateral area of a single nanosheet is recorded as A. Therefore, the surface energy contributed by the area immersed in the gas phase is calculated from Eq. (15):

$$\Delta E_{sg} = A \times \gamma_{sg} \tag{15}$$

The surface energy contributed by the area immersed in the water phase is calculated from Eq. (16):

$$\Delta E_{sw} = A \times \gamma_{sw} \tag{16}$$

The surface energy contributed by the eliminated gas–water surface owing to the presence of a single nanosheet is obtained from Eq. (17):

$$\Delta E_{gw} = A \times \gamma_{gw} \tag{17}$$

Hence, the required energy to remove the adsorbed single nanosheet to the water phase can be determined according to Eq. (18):

$$\Delta G = \Delta E_{sw} - \Delta E_{sg} + \Delta E_{gw} = A \times \left(\gamma_{sw} - \gamma_{sg} + \gamma_{gw}\right) \tag{18}$$

According to Young Eq. (12), Eq. (18) can be simplified to Eq. (19):

$$\Delta G = A\gamma_{gw}(1-\cos\theta) \tag{19}$$

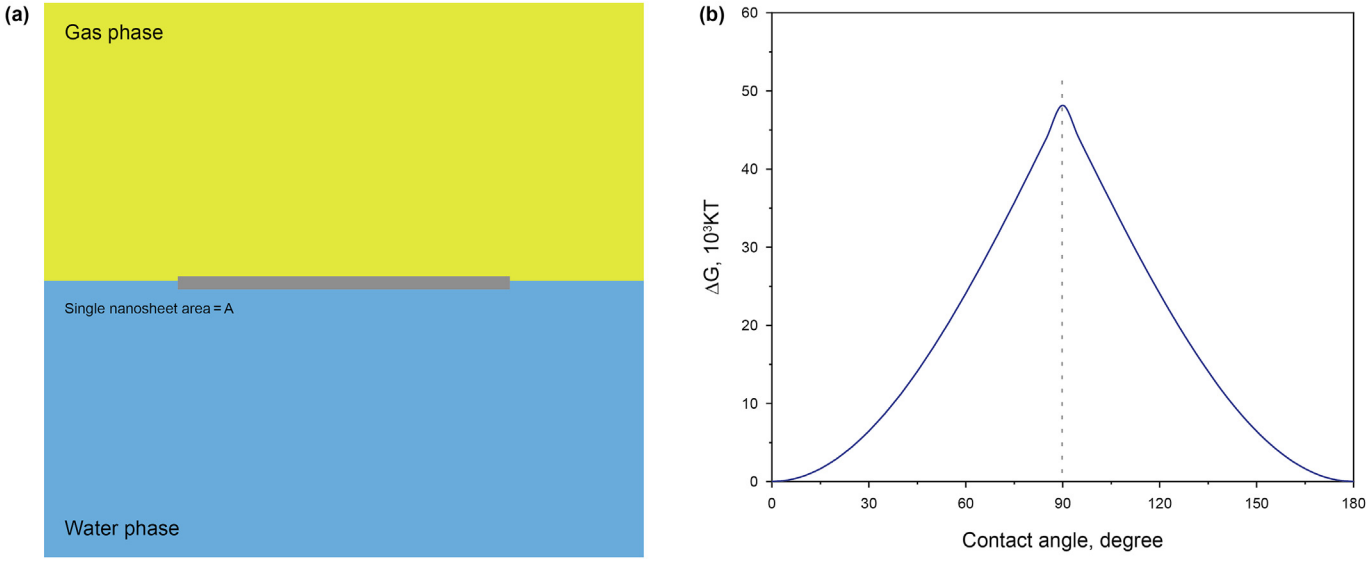

Fig. 9. **a** A single nanosheet adsorbed at the gas-water surface, **b** desorption energy of a specific nanosheet.

Similarly, the required energy to remove the adsorbed single nanosheet to the gas phase can be determined according to Eq. (20):

$$\Delta G = A\gamma_{gw}(1+\cos\theta) \tag{20}$$

According to Eqs. (19) and (20), the desorption energy of s single nanosheet from the surface to the bulk phase is calculated and drawn in Fig. 9b as a function of the contact angle of the nanosheet surface. Several parameters of nanosheet size (Length, 60 nm), surface tension (γ_{gw}, 55 mN/m), and temperature (298 K) are given to calculate a single nanosheet's desorption energy. It concludes that the maximum desorption energy is achieved as the contact angle is 90°. Compared to a single spherical nanoparticle (R, 30 nm), a single nanosheet requires more desorption energy to get rid of the surface. This result signifies that nanosheets show a promising prospect for improving foam stability.

4.4. Emulsion stabilization improvement

Numerous literature and pilot plant studies confirm that oil recovery can be improved through crude oil emulsification. Several mechanisms, like micro displacement efficiency improvement, macro sweep efficiency improvement, and oil viscosity reduction (oil in water emulsion), are used to verify such phenomenon (Guo et al., 2018; Karambeigi et al., 2015; Li et al. 2018b, 2019b; Ning et al., 2018). Chen et al. (2013) reported that higher oil recovery can be achieved when improving emulsification ability. Moreover, emulsions were also used to block pores during steam flooding (French et al., 1986). Therefore, improvement of emulsion stability is necessary during the emulsion migration process under harsh reservoir conditions.

Over the decades, Pickering emulsions stabilized by particles have gained considerable attraction for EOR due to their advantages in improving emulsion stability over conventional surfactant emulsion (Tyowua et al., 2017; Zhang et al., 2018). Nanoparticles can improve emulsion stability by forming single or multilayered nanoparticle interfacial films at the oil-water interface (Stancik et al., 2004). The mechanical strength and viscoelasticity of interfacial film can be improved by the adsorption of nanoparticles, preventing oil droplets from deformation and collision coalescence (Li et al., 2019b; Tambe and Sharma, 1995). Modified gold nanoparticles and alkane were evenly mixed to form O/W emulsions, which were still stable during performed cooling-heating cycles (Kubowicz et al., 2010). Additionally, adsorption behaviors of soy protein isolate-chitosan nanoparticles (SPI-CS) at Pickering emulsion interfaces were characterized using confocal laser scanning microscopy (CLSM), as shown in Fig. 10 (Yang et al., 2020). The SPI-CS nanoparticles and corn oil were dyed with Nile blue (red) and Nile red (green) to enhance the experiments' visual effect. It can be intuitively observed that SPI-CS nanoparticles were tightly adsorbed at the oil-water interfaces, forming nanoparticles interfacial film to prevent coalescence of adjacent oil droplets. Moreover, Koroleva and Yurtow (2020) systematically studied Pickering emulsions' stability with magnetite/silica and gold/silica nanoparticles using experimental and mathematical modeling. Experimental results demonstrated that Pickering emulsions stabilized by magnetite/silica nanoparticles can prevent emulsions from coalescence. It also confirms that silica and magnetite nanoparticles can be adsorbed onto the oil-water interface to form chain-like heteroaggregates extended into the bulk aqueous phase. The formation of 3-D gel-like network around oil droplets is beneficial to inhibit their demulsification and coalescence. Once the nanoparticles get adsorbed onto the oil-water interfaces, it is difficult to be detached from the interface. The required desorption energy can be calculated based on Eqs. (13), (14), (19) and (20) just using the relevant oil-water interface parameters instead of gas-water parameters.

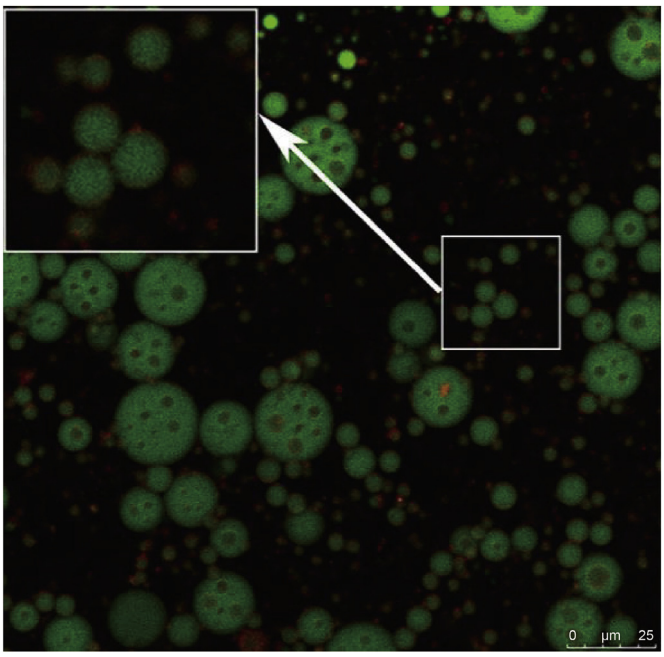

Fig. 10. CLSM image of Pickering emulsions stabilized by SPI-CS nanoparticles (Yang et al., 2020).

4.5. Structural disjoining pressure

Over the decades, nanofluid has been a promising candidate for enhanced oil recovery. The conventional C-EOR mechanisms cannot be used to interpret the faster spreading velocity of nanoparticles on the solid surfaces during the nanofluid flooding process. Such behaviors of nanoparticles occur due to the formation of disjoining pressure in the confinement of the three-phase contact region formed by an oil drop on a solid surface. The disjoining pressure is contained by van der Waals's force (Gennes, 1985). Hirasaki (1991) proposed that the disjoining pressure is a combination of electrostatic forces and van der Waals' force. The above two kinds of conventional disjoining pressures (CDP) are generated due to the London–Van der Waals force with a short-range nature. However, the most popular theory is the concept of structural disjoining pressure (SDP). Recently, Wassan and Nikolov (Wasan and Nikolov, 2003) proposed the concept of SDP, which is a kind of force normal to the interface with long-range nature. The formation of SDP results from spherical nanoparticles' ordering in a confining region (wedge film). In other words, the origin of SDP is due to the confinement of nanoparticles at the wedge film structure instead of the freedom nanoparticles in the bulk phase. The wedge-film depth can be extended from one nanoparticle to several nanoparticle diameters along the direction of the opening of the wedge film. An analytical expression (Trokhymchuk et al., 2001) for calculating SDP based on a solution of the Ornstein-Zernike statistical mechanics is showed in the following Eqs:

$$\Pi_{st}(h) = -P,\ 0<h<d \tag{21}$$

$$\Pi_{st}(h) = \Pi_0\cos(\omega h+\varphi_2)e^{-kh} + \Pi_1 e^{-\delta(h-d)},\ h>d \tag{22}$$

Where d is the diameter of nanoparticle, h is the wedge film

thickness, and all other parameters (Π_0, Π_1, ω, φ_2, κ, δ) in Eq. (22) are fitted as cubic polynomials in terms of the nanofluid volume fraction (φ). P is the osmotic pressure, which is a function of the nanofluid volume fraction, as shown in Eq. (23):

$$P = \rho k T \frac{1 + \varphi + \varphi^2 - \varphi^3}{(1 - \varphi)^3} \tag{23}$$

Where,

$$\varphi = \frac{6 n_p}{\pi d^3} \tag{24}$$

Here, n_p is the number of particles per unit volume of the system.

Known from Eqs. (21)–(24), the osmotic and structural disjoining pressures at the confinement region increase by increasing the nanoparticles' volume fraction. The volume fraction is inversely proportional to the diameter of a nanoparticle. The SDP depends on the nanoparticle diameter, temperature, volume fraction, and other nanoparticles' properties. Moreover, the absolute value of structural disjoining pressure is equal to that of osmotic pressure when the wedge film depth is less than the nanoparticle diameter. The higher the osmotic pressure, the higher the SDP. The above results are verified by the mathematical models of Chengara (Chengara et al., 2004).

The SDP presents an oscillatory decay profile with the increase of film thickness from vertex to bulk phase. The highest SDP at the vertex of wedge film reaches 50000 Pa and enhances nanofluid spreading. Meanwhile, the spreading of nanoparticles on the solid surface can change the solid surface's wettability from oil-wet to neutral-wet or water-wet. As a result, the oil drop trapped within reservoir pores and throats can be gradually detached by the wedge film's moving forward. Recently, ShamsiJazeyi et al. (2014) pointed out that the structural disjoining pressure contained four components: SDP, van der Waals, electrostatic, and solvation forces. Those affect the detached process of oil drop from a solid surface to the bulk phase. In particular, the ability of wettability alteration can be virtually affected by the electrostatic force of nanoparticles. An increase in electrostatic repulsive forces on the surface of the nanoparticles can increase the disjoining pressure, which leads to the spreading of nanofluid on the solid surface, followed by detaching the oil drop from the solid surface.

Affected by structural disjoining pressure, the confinement region between oil drop, solid surface, and the water phase is distinct at nanoparticles' presence or absence. Two distinct contact lines (Fig. 11): an outer one (among the oil droplet, solid, and water film) and an inner one (among the oil droplet, solid, and a mixed oil-water film) were observed when seen from the top of oil drop (Kondiparty et al., 2012). The outer contact line represents the conventional three-phase contact line, while the inner line is the boundary where the spreading edge of the nanofluid film and the oil-solid interface meet. The inner contact line is formed and gradually moves towards the center of the contact region between the oil drop and solid surface due to nanoparticles' presence. This spreading behavior of nanofluid is driven by the net spreading force, which is defined as the difference between the film tension gradient (structural disjoining pressure gradient) arising from the structuring of the nanoparticles in the wedge confinement and the contribution from the resisting capillary and hydrostatic pressures (the buoyancy because the drop is sessile). Moreover, the nanofluid film's spreading speed on the solid surface increases with an increase in nanoparticle concentration and oil drop volume.

Wasan and Nikolov (2003) observed the formation of a two-dimensional (2D) colloidal crystal structure in the wedge film when the wedge film thickness was less than twice the nanoparticle's diameter. As the thickness of wedge film is more than three times the nanoparticle's diameter, nanoparticles'

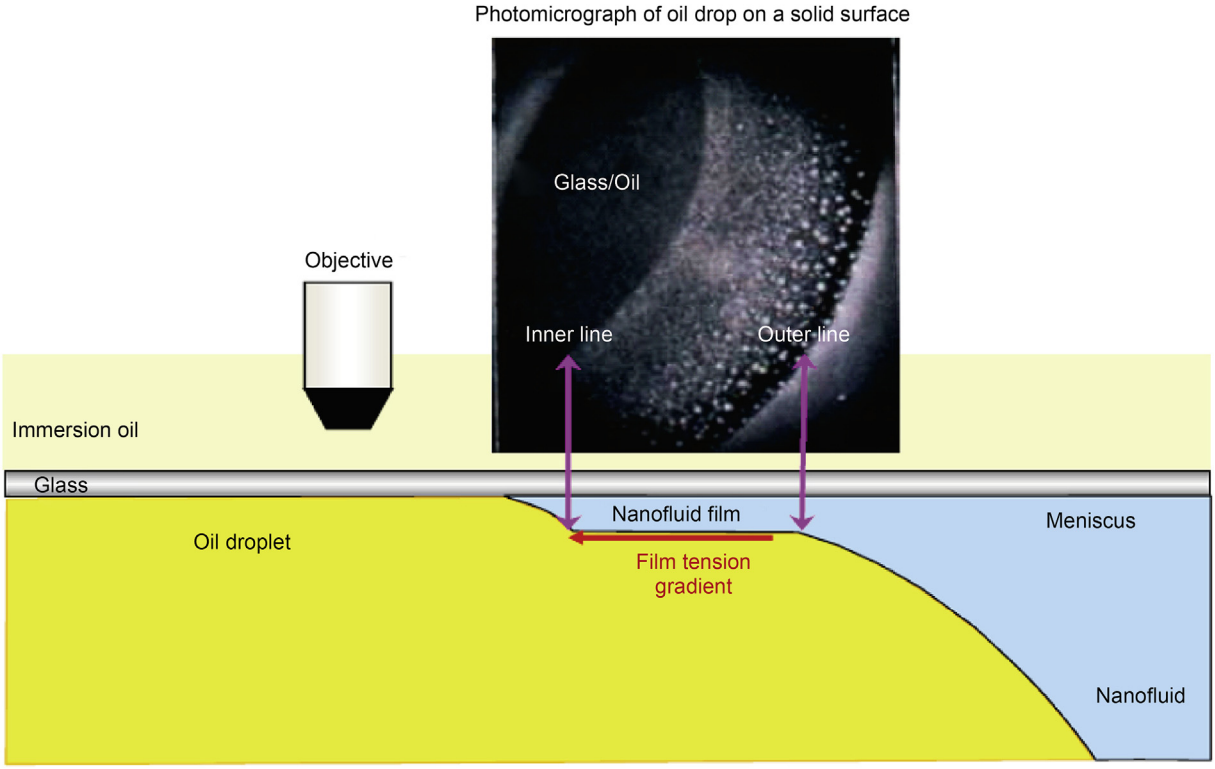

Fig. 11. Photomicrograph taken using reflected-light interferometry depicting the inner and outer contact lines and the nanofluid film region (Kondiparty et al., 2012).

arrangement in the wedge-film structure becomes disordered. The vertex of wedge film can generate high disjoining pressure (nearly 50 kPa), promoting the wedge film moving forward and the nanoparticles spreading on the solid surface. With the lapse of time, the oil drop trapped on the solid surface is detached.

Zhang et al. (2014) investigated the dewetting phenomenon of the simulated oil film in a glass capillary in the presence of nanoparticles, as shown in Fig. 12. The thick oil film formed after nanofluid driven is unstable and broken to form an oil annular rim. Finally, the annular rim is detached from the solid surface to form a spherical oil droplet due to nanoparticles' arrangement in the wedge-film region. The observed phenomenon is repeatable. As a result, the nanofluid can be widely applicable in extracting crude oil film from the rock surface during N-EOR.

However, it should be noted that the formation of SDP at the confinement structure (wedge film) can be regarded as one of the mechanisms for N-EOR when the volume fraction of nanoparticles is more than 20 v% (Kondiparty et al., 2012; Wasan and Nikolov, 2003). The dewetting phenomenon occurred at the capillary tube when the volume fraction of SiO_2 was 20 v%. On the other hand, Chengara et al. (2004) found that the contact line's position had no appreciable change when the volume fraction of nanoparticles was less than 20 v%. Those results demonstrate that nanofluids can only play positive effects on removing residual oil from a solid surface when the nanoparticles volume fraction is more than 20 v%. However, many N-EOR experiments were conducted at a very dilute concentration of nanoparticles in the literature (Hu et al., 2016; Li et al., 2018a). Therefore, it is worthy of studying whether the structural disjoining pressure arising from the confinement wedge film region during N-EOR flooding can interpret the residual oil removal process from the rock surface when the concentration of nanoparticles is low. Moreover, the above phenomena and Eqs are investigated and obtained when using spherical nanoparticles. The critical volume fraction (20 v%) may be decreased when using nanosheets due to their flake-like shape (Qu et al., 2021).

4.6. Depressurization and increasing injection

More oil reserve has been stored in low permeability reservoirs (permeability 0.1 to 50 mD). Micron or nano-sized pores and throats are widely distributed in low permeability reservoirs, resulting in the higher injection pressure of displacing fluid and lower oil recovery (Cheng et al., 2006). Hence, it is necessary to reduce injection pressure and increase injection for high-efficiency developing low permeability reservoirs.

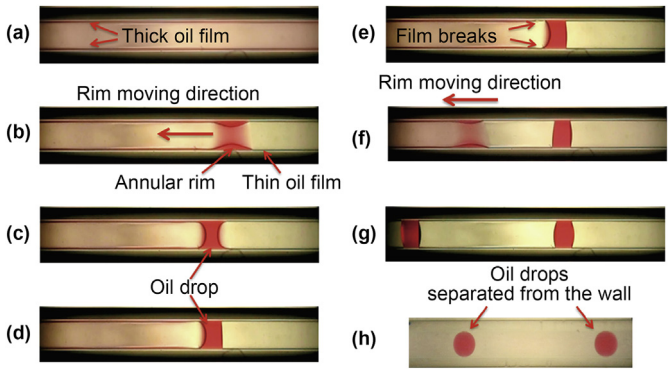

Fig. 12. Evolution of hexadecane film inside the glass capillary (ID = 282 ± 2 μm), **(a)** thick film after nanofluid driven, **(b)** dewetting of the thick film in the form of the annular rim, **(c)** formation of double-concave meniscus across the capillary, **(d)** rupture of the thin film on the right side of the meniscus, **(e-g)** repeats the previous steps and forms a cylindrical drop, **(h)** separation of cylindrical drops from the capillary wall by the nanofluid (Zhang et al., 2014).

Recently, nanofluids have been considered a kind of drag reduction agent. Polesil, a kind of pressure-decreasing and augmented injection agent consisting of nanoparticles, was firstly applied in China (Lau et al., 2017). However, the effects of nanofluids applied in pilots were not very satisfactory owing to various reasons. Yu et al. (2020) reported that micro-emulsion-based silicon nanofluids can reduce the water injection pressure to more than 40% at the silica concentration of 1 wt%. Modified silicon dioxide (SiO_2) was also prepared to achieve the highest pressure drop rate (34%) when the injection volume was less than 0.3 times the pore volume (PV) (Hai et al., 2020). Initially, the mechanism for applying nano-silicon dioxide (SiO_2) in the pressure drop and enhancing water injection technology can be expressed as the nano-adsorption layer replaces the hydration layer on the rock surface, and then pore diameter is increased (Li et al., 2017a; Wasan and Nikolov, 2003). However, the hydration layer height is found to be around 5–30 nm at driven pressure of 0.01–2 MPa, which is the same order of magnitude as the nanoparticle size (He and Hua, 1998). Hence, this interpretation may not be suitable for depressurization and increasing injection technology. Cottin-Bizonne et al. (2003) found that the synergistic effects of wettability and roughness of rock surface can significantly decrease the flow resistance of fluids in pores and throats. Di et al. (2007) proposed another mechanism for interpreting depressurization and increasing injection. He thought that hydrophobic nanoparticles can adsorb onto the rock surface to form nanoparticle layers instead of replacing a hydrated layer. The slip effects of nanoparticles can significantly decrease the flow resistance and then increase injection. The micro-tube was designed to study the impact of nanofluids injection rate and pore size distributions on pressure reduction (Wang et al., 2018). Experimental results exhibited that hydrophobic nanoparticles showed greatly pressure-decreasing ability, first increased and then decreased with the injection rate increases, as shown in Fig. 13. The results can be attributed to that the adsorption of hydrophobic nanoparticles improves rock surface roughness.

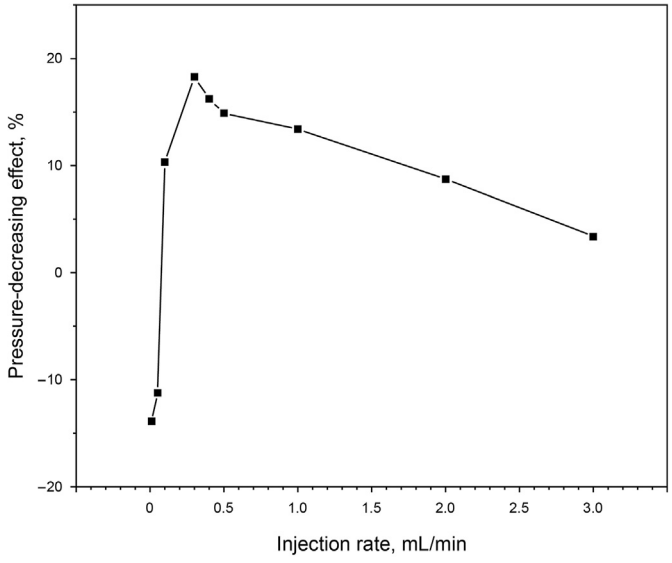

Fig. 13. Effects of injection rate on pressure-decreasing when using microtube (Wang et al., 2018).

5. Nano-assisted C-EOR

Recently, C-EOR and N-EOR technologies are two major branches to enhance oil recovery. Many reviews focus on the synergism of C-EOR and N-EOR technologies (nano-assisted C-EOR) (Cheraghian and Hendraningrat, 2016; Kamal et al., 2017; Negin et al., 2016). For instance, combinations of nanoparticles and polymers are manipulated to improve the properties of pure polymer solutions, such as thermal stability, viscoelasticity, and mechanical stability. Taborda et al. (2021) reported that polymer solution's thermal stability and viscosity retention can be significantly improved by introducing nanoparticles, resulting in an excellent mobility ratio during the polymer flooding process. Kang et al. (2019) also had mixed the silica nanoparticles and amphiphilic polymer to form an NP-polymer composite under high temperature and high salinity conditions. Results showed that the polymer solution's apparent viscosity and viscoelasticity were significantly increased after silica NPs addition (Fig. 14). The synergistic effect of titanium dioxide NPs (optimal concentration, 2.3 wt%) and HPAM polymer solution was also evaluated to mobilize dead oil from sandstone core samples (Cheraghian and Goshtasp, 2016a). Results revealed that improved oil recovery was ascribed to the improvement of viscosity after TiO_2 addition.

Apart from NP-polymer synergism, NP-surfactant synergism has also been widely studied for further changing interfacial properties (Munshi et al., 2008). The mixtures of surfactants and NPs can further lead to IFT reduction, wettability alteration, oil viscosity reduction, foam/emulsion stability improvement, and capillary force decrease (Ravera et al., 2006; Rosen et al., 2005). A novel nanofluid was prepared by combining the positively charged amino-terminated silica nanoparticles ($SiNP-NH_2$) with a negatively charged anionic surfactant (Soloterra 964) via electrostatic force (Zhou et al., 2019). Results proved that oil-water interfacial tension was decreased by 99.85%, and the contact angle was increased by 237.8% over the original value of 13.78 mN/m and 43.4°, respectively. The interfacial tension of the oil-brine system was decreased from 19 to 8 mN/m after introducing SiO_2 nanoparticles (Hendraningrat et al., 2013). Moreover, more than 13% of heavy oil recovery was achieved using the mixture of SDS/SiO_2 NPs compared to SDS alone (Cheraghian et al., 2017). The oil recovery improvement can be attributed to the increased viscosity of the displacing phase. Many similar results, including IFT reduction and wettability alteration from oil-wet to water-wet after introducing nanoparticles, were also reported by other published papers (Ahmed et al., 2018; Al-Anssari et al., 2017; Cheraghian and Goshtasp, 2016b; Parvazdavani et al., 2014).

6. Current challenges and future prospects of nanoparticles for N-EOR

Although many nanoparticles (SiO_2, CuO, MoS_2, etc.) have been successfully studied to enhance oil recovery in the laboratory, there are still many concerns limiting their applications from laboratory scale to field scale. This section discusses the current challenges and future prospects faced by nanoparticles in EOR.

6.1. Improvement of nanofluid stability

Nanoparticles are often used to enhance oil recovery in the form of nanofluid. The dispersion degree of nanoparticles in a specifically based fluid has been affected by temperature, salinity, based fluid properties (alcohol, water), nanoparticles' surface properties, etc. Once unstable nanofluid is injected into complex reservoirs, the solid nanoparticles tend to aggregate or deposit to form a large size cluster, resulting in damage to reservoir permeability and pores and throats structures. Hence, nanofluid stability improvement, especially under harsh reservoir conditions (high temperature, high salinity and etc.), should be considered before following properties evaluation.

6.2. Improvement of surface activity of nanoparticles

Amphiphilic (Janus) nanoparticles with hydrophilic and lipophilic nature show excellent properties for EOR over SHNPs. As a kind of solid surfactant, amphiphilic nanoparticles can significantly reduce interfacial tension, self-adsorb onto the interface, and

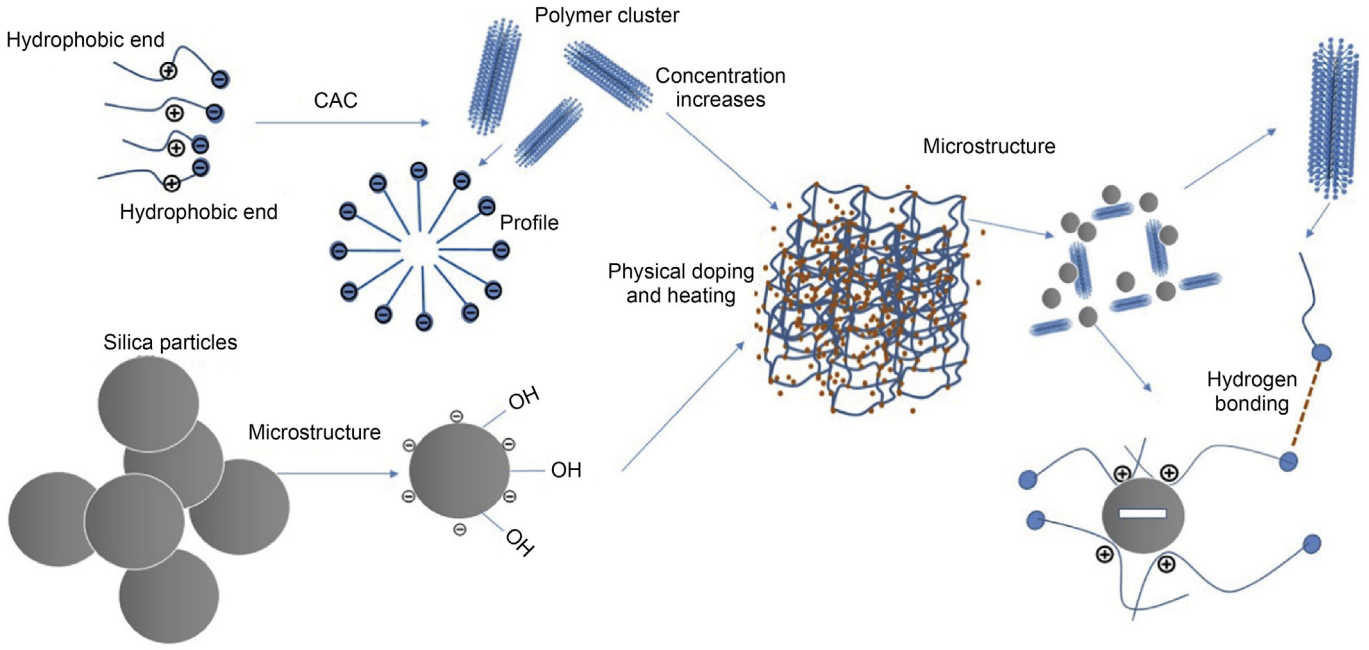

Fig. 14. Mechanism of silica NPs to improve amphiphilic polymer viscosity (Kang et al., 2019).

change interface properties. Commonly, the SHNPs possessing single wettability (hydrophilic or hydrophobic) tend to disperse into the bulk phase instead of interfaces and have no apparent contributions to interface properties. Therefore, amphiphilic nanoparticles are superior to SHNPs for N-EOR.

6.3. Clarification in EOR mechanisms and flow in porous media of nanofluids

Apart from interfacial tension reduction, wettability alteration, and foam/emulsion stability improvement, nanofluid's unique oil displacement mechanism is the generation of structural disjoining pressure in the confinement structure (wedge film). However, as mentioned above, this structural disjoining pressure occurs when the volume fraction of used spherical nanoparticles is more than 20 v%. Therefore, we should urgently reveal the mechanisms for oil displacement during the N-EOR process while using nanofluid. Moreover, can the critical value for volume fraction (20 v%) be decreased when using nanosheets?

Another concern limiting nanofluid application to field scale is the flow in porous media of nanofluid during N-EOR. There is no definite answer for adding solid nanoparticles to the water phase to affect the flow in porous media of the water phase, such as the relative permeability curve.

6.4. Production cost reduction of nanofluid

Lastly, there are many ways to prepare various nanofluids. However, it is necessary to reduce nanofluids' production costs as the oil price decreases, which is also the economic premise for the broad application of nanofluids from laboratory scale to field scale.

As the price of chemicals is increasing, nanofluid oil displacement technology (N-EOR) can replace traditional chemical oil displacement technology (C-EOR) in the future due to the numerous advantages of nanoparticles and the relatively low production cost. Over the decades, SiO_2 nanoparticles are the most widely used nanomaterial to boost EOR. However, using different nanomaterials instead of regular spherical nanoparticles may yield better results in EOR due to their unique physical and chemical properties.

7. Conclusion

This work summarizes the most recent progress of nanoparticles used as nanofluids for enhancing oil recovery. Here, we mainly summarize the preparation methods of amphiphilic nanoparticles for the crude oil development, followed by the evaluation techniques for nanofluid stability. The mechanisms of nanofluids during N-EOR processes in terms of interfacial tension reduction, wettability alteration, foam stabilization, emulsion stabilization, structural disjoining pressure, and depressurization-increasing injection are also discussed and reviewed. Compared to SHNPS, the amphiphilic nanomaterials show great potential in improving oil recovery. However, there is much literature focusing on the applications of nanofluids for oil recovery at the laboratory level, but the successful field applications are few. Besides, we also summarize the limitations on their applications from laboratory scale to field scale in terms of large-scale production, lower production cost, and surface properties improvement. Such difficulties can be overthrown by improving the synthesis techniques. Thereby, the nanofluid can still be regarded as an outstanding candidate for enhancing oil recovery significantly in the future.

Acknowledgments

The authors gratefully appreciate the financial support of the Science Foundation of China University of Petroleum, Beijing (Grant No. 2462020XKBH013). Financial supports from the National Natural Science Foundation of China (Grant No. 51804316) and the Science Foundation of China University of Petroleum, Beijing (Grant No. 2462017YJRC037) are also significantly acknowledged. Finally, Tuo Liang wants to thank the invaluable care and support from Jiaxin Xi (my wife) over the years. You are the world to me.

References

Abidin, A.Z., Puspasari, T., Nugroho, W.A., 2012. Polymers for enhanced oil recovery technology. Procedia Chem. 4, 11–16. https://doi.org/10.1016/j.proche.2012.06.002.

Aftab, A., Ismail, A.R., Ibupoto, Z.H., et al., 2017. Nanoparticles based drilling muds a solution to drill elevated temperature wells: a review. Renew. Sustain. Energy Rev. 76, 1301–1313.

Afzalitabar, M., Alaei, M., Bazmi, M., et al., 2017. Facile and economical preparation method of nanoporous graphene/silica nanohybrid and evaluation of its Pickering emulsion properties for Chemical Enhanced oil Recovery (C-EOR). Fuel 206, 453–466. https://doi.org/10.1016/j.fuel.2017.05.102.

Agi, A., Junin, R., Jaafar, M.Z., et al., 2021. Formulation of bionanomaterials: a review of particle design towards oil recovery applications. J. Ind. Eng. Chem. 98, 82–102. https://doi.org/10.1016/j.jiec.2021.03.032.

Ahmed, A., Mohd, S.I., Rashidah, P.P., et al., 2018. Development of surface treated nanosilica for wettability alteration and interfacial tension reduction. J. Dispersion Sci. Technol. 1–7. https://doi.org/10.1080/01932691.2017.1417133.

Ahmed, T., 2010. Chapter 11 - oil recovery mechanisms and the material balance equation. In: Ahmed, T. (Ed.), Reservoir Engineering Handbook, fourth ed. Gulf Professional Publishing, Boston, pp. 733–809.

Al-anssari, S., Nwidee, L.N., Arif, M., et al., 2017. Wettability Alteration of Carbonate Rocks via Nanoparticle-Anionic Surfactant Flooding at Reservoirs Conditions, SPE Symposium: Production Enhancement and Cost Optimisation, vol. 12. Society of Petroleum Engineers, Kuala Lumpur, Malaysia. https://doi.org/10.2118/189203-MS.

Ali, H., Soleimani, H., Yahya, N., et al., 2020. Enhanced oil recovery by using electromagnetic-assisted nanofluids: a review. J. Mol. Liq. 309, 113095. https://doi.org/10.1016/j.molliq.2020.113095.

Aliu, O., Sakidin, H., Foroozesh, J., et al., 2020. Lattice Boltzmann application to nanofluids dynamics-A review. J. Mol. Liq. 300, 112284. https://doi.org/10.1016/j.molliq.2019.112284.

Alnarabiji, M.S., Husein, M.M., 2020. Application of bare nanoparticle-based nanofluids in enhanced oil recovery. Fuel 267, 117262. https://doi.org/10.1016/j.fuel.2020.117262.

Alnarabiji, M.S., Yahya, N., Nadeem, S., et al., 2018. Nanofluid enhanced oil recovery using induced ZnO nanocrystals by electromagnetic energy: viscosity increment. Fuel 233, 632–643. https://doi.org/10.1016/j.fuel.2018.06.068.

Alyousef, Z.A., Almobarky, M., Schechter, D.S., 2017. Enhancing the stability of foam by the use of nanoparticles. Energy Fuel. 31 (10), 10620–10627. https://doi.org/10.1021/acs.energyfuels.7b01697.

Aveyard, R., Binks, B.P., Clint, J.H., 2003. Emulsions stabilised solely by colloidal particles. Adv. Colloid Interface Sci. 100, 503–546. https://doi.org/10.1016/S0001-8686(02)00069-6.

Bahraminejad, H., Manshad, A.K., Riazi, M., et al., 2019. CuO/TiO_2/PAM as a novel introduced hybrid agent for water—oil interfacial tension and wettability optimization in chemical enhanced oil recovery. Energy Fuel. 33 (11), 10547–10560. https://doi.org/10.1021/acs.energyfuels.9b02109.

Binks, B.P., Lumsdon, S.O., 2000. Influence of particle wettability on the type and stability of surfactant-free emulsions. Langmuir 16 (23), 8622–8631. https://doi.org/10.1021/la000189s.

Biswal, N.R., Singh, J.K., 2016. Interfacial behavior of nonionic Tween 20 surfactant at oil–water interfaces in the presence of different types of nanoparticles. RSC Adv. 6 (114), 113307–113314. https://doi.org/10.1039/C6RA23093H.

Bukar, N., Zhao, S.S., Charbonneau, D.M., et al., 2014. Influence of the Debye length on the interaction of a small molecule-modified Au nanoparticle with a surface-bound bioreceptor, 50, pp. 4947–4950. https://doi.org/10.1039/c4cc01423e, 38.

Cacua, K., Ordonez, F., Zapata, C., et al., 2019. Surfactant concentration and pH effects on the zeta potential values of alumina nanofluids to inspect stability. Colloid. Surface. Physicochem. Eng. Aspect. 583, 123960. https://doi.org/10.1016/j.colsurfa.2019.123960.

Chakraborty, S., Panigrahi, P.K., 2020. Stability of nanofluid: a review. Appl. Therm. Eng. 174, 115259. https://doi.org/10.1016/j.applthermaleng.2020.115259.

Chakraborty, S., Sarkar, I., Ashok, A., et al., 2018. Synthesis of Cu-Al LDH nanofluid and its application in spray cooling heat transfer of a hot steel plate. Powder Technol. 335, 285–300. https://doi.org/10.1016/j.powtec.2018.05.004.

Chakraborty, S., Sarkar, I., Behera, D.K., et al., 2017. Experimental investigation on the effect of dispersant addition on thermal and rheological characteristics of TiO_2 nanofluid. Powder Technol. 307, 10–24. https://doi.org/10.1016/j.powtec.2016.11.016.

Chen, L., Zhang, G., Ge, J., et al., 2013. Research of the heavy oil displacement mechanism by using alkaline/surfactant flooding system. Colloid. Surface. Physicochem. Eng. Aspect. 434, 63–71. https://doi.org/10.1016/j.colsurfa.2013.05.035.
Chen, L.F., Xie, H.Q., 2010. Properties of carbon nanotube nanofluids stabilized by cationic gemini surfactant. Thermochim. Acta 506 (1–2), 62–66. https://doi.org/10.1016/j.tca.2010.04.016.
Chengara, A., Nikolov, A.D., Wasan, D.T., et al., 2004. Spreading of nanofluids driven by the structural disjoining pressure gradient. J. Colloid Interface Sci. 280 (1), 192–201. https://doi.org/10.1016/j.jcis.2004.07.005.
Cheng, Y.M., Li, X.H., Li, Q.H., et al., 2006. Preparation and performance of water-based nanometer polysilicon as augmented injection for oil field. Chem. Res. (4), 56–59. https://doi.org/10.3969/j.issn.1008-1011.2006.04.017.
Cheraghian, G., 2016a. Effect of nano titanium dioxide on heavy oil recovery during polymer flooding. Petrol. Sci. Technol. https://doi.org/10.1080/10916466.2016.1156125.
Cheraghian, G., 2016b. Effects of titanium dioxide nanoparticles on the efficiency of surfactant flooding of heavy oil in a glass micromodel. Petrol. Sci. Technol. 34 (3), 260–267. https://doi.org/10.1080/10916466.2015.1132233.
Cheraghian, G., Hendraningrat, L., 2016. A review on applications of nanotechnology in the enhanced oil recovery part A: effects of nanoparticles on interfacial tension. Int. Nano Lett. 6 (2), 129–138. https://doi.org/10.1007/s40089-015-0173-4.
Cheraghian, G., Kiani, S., Nassar, N.N., et al., 2017. Silica nanoparticle enhancement in the efficiency of surfactant flooding of heavy oil in a glass micromodel. Ind. Eng. Chem. Res. 56 (30), 8528–8534. https://doi.org/10.1021/acs.iecr.7b01675.
Cottin-bizonne, C., Barrat, J.L., Bocquet, L., et al., 2003. Low-friction flows of liquid at nanopatterned interfaces. Nat. Mater. 2 (4), 237–240. https://doi.org/10.1038/nmat857.
Defolter, J.W.J., Hutter, E.M., Castillo, S.I.R., et al., 2014. Particle shape anisotropy in pickering emulsions: cubes and peanuts. Langmuir 30 (4), 955–964. https://doi.org/10.1021/la402427q.
Di, Q.F., Gu, C.Y., Shi, L.Y., et al., 2007. PRESSURE DROP MECHANISM OF ENHANCING WATER INJECTION TECHNOLOGY WITH HYDROPHOBICITY NANOMETER SiO_2. Drill. Prod. Technol. (4), 91–94+3. CNKI:SUN:ZCGY.0.2007-04-031.
Dehghan, M.A., Ghazanfari, M.H., 2019. Wettability alteration of oil-wet carbonate porous media using silica nanoparticles: electrokinetic characterization. Ind. Eng. Chem. Res. 58 (40), 18601–18612. https://doi.org/10.1021/acs.iecr.9b03060.
Du, K., Glogowski, E., Emrick, T., et al., 2010. Adsorption energy of nano- and microparticles at liquid-liquid interfaces. Langmuir 26 (15), 12518–12522. https://doi.org/10.1021/la100497h.
Esfandyari, B.A., Radzuan, J., Shahaboddin, S., et al., 2015. Transport and retention of engineered Al_2O_3, TiO_2, and SiO_2 nanoparticles through various sedimentary rocks. Sci. Rep. 5. https://doi.org/10.1038/srep14264.
Esfandyari, H., Shadizadeh, S.R., Esmaeilzadeh, F., et al., 2020. Implications of anionic and natural surfactants to measure wettability alteration in EOR processes. Fuel 278, 118392. https://doi.org/10.1016/j.fuel.2020.118392.
Esmaeilzadeh, P., Hosseinpour, N., Bahramian, A., et al., 2014. Effect of ZrO_2 nanoparticles on the interfacial behavior of surfactant solutions at air–water and n-heptane–water interfaces. Fluid Phase Equil. 361, 289–295. https://doi.org/10.1016/j.fluid.2013.11.014.
Farahmandjou, M., Sebt, S.A., Parhizgar, S.S., et al., 2009. Stability investigation of colloidal FePt nanoparticle systems by spectrophotometer analysis. Chin. Phys. Lett. 26 (2). https://doi.org/10.1088/0256-307X/26/2/027501.
Fatehah, M.O., Hamidi, A.A., Serge, S., 2014. Stability of ZnO nanoparticles in solution. Influence of pH, dissolution, aggregation and disaggregation effects. J. Colloid Sci. Biotechnol. 3 (1). https://doi.org/10.1166/jcsb.2014.1072.
Fereidooni, M.T., Azizian, S., 2014. Effect of ZnO nanoparticle and hexadecyltrimethylammonium bromide on the dynamic and equilibrium oil–water interfacial tension. J. Phys. Chem. B 118 (6), 1527–1534. https://doi.org/10.1021/jp4106986.
Foroozesh, J., Kumar, S., 2020. Nanoparticles behaviors in porous media: application to enhanced oil recovery. J. Mol. Liq. 316, 113876. https://doi.org/10.1016/j.molliq.2020.113876.
French, R.A., Jacobson, A.R., Kim, B., et al., 2009. Influence of ionic strength, pH, and cation valence on aggregation kinetics of titanium dioxide nanoparticles. Environ. Sci. Technol. 43 (5), 1354–1359. https://doi.org/10.1021/es802628n.
French, T.R., Broz, J.S., Lorenz, P.B., et al., 1986. Use of Emulsions for Mobility Control during Steamflooding, SPE California Regional Meeting, vol. 12. Society of Petroleum Engineers, Oakland, California. https://doi.org/10.2523/15052-MS.
Gao, H.M., Lu, Z.Y., Liu, H., 2014. Orientation and surface activity of Janus particles at fluid-fluid interfaces, 141, 134907. https://doi.org/10.1063/1.4897185, 13.
Gennes, P.G.D., 1985. Wetting: static and dynamics. Rev. Mod. Phys. 57. https://doi.org/10.1103/RevModPhys.57.827.
Gomez, F.A., Bradford, S.A., Hwang, G., et al., 2020. Shape and orientation of bare silica particles influence their deposition under intermediate ionic strength: a study with QCM–D and DLVO theory. Colloid. Surface. Physicochem. Eng. Aspect. 599, 124921. https://doi.org/10.1016/j.colsurfa.2020.124921.
Guo, Y.B., Yue, X.A., Fu, J.Y., et al., 2018. Relevance between emulsification capability and interfacial tension of chemical flooding agents. Energy Fuel. 32 (12), 12345–12350. https://doi.org/10.1021/acs.energyfuels.8b03110.
Hadia, N.J., Ng, Y.H., Stubbs, L.P., et al., 2021. High Salinity and High Temperature Stable Colloidal Silica Nanoparticles with Wettability Alteration Ability for EOR Applications. https://doi.org/10.3390/nano11030707.
Hai, X.H., J, Z., D, L.L., 2020. Preparation of functional nanofluid dispersion and reduction of water injection pressure. Sci. Technol. Eng. 20 (16), 6429–6432. https://doi.org/10.3969/j.issn.1671-1815.2020.16.018.
Hajiabadi, S.H., Aghaei, H., Kalateh, A.M., et al., 2020. An overview on the significance of carbon-based nanomaterials in upstream oil and gas industry. J. Petrol. Sci. Eng. 186, 106783. https://doi.org/10.1016/j.petrol.2019.106783.
He, C.Z., Hua, M.Q., 1998. The thickness of water-film in oil and gas reservoirs. Petrol. Explor. Dev. 25 (2), 75–77. CNKI:SUN:SKYK.0.1998-02-022.
Heinz, H., Chandrani, P., Ozge, H., et al., 2017. Nanoparticle decoration with surfactants: molecular interactions, assembly, and applications. Surf. Sci. Rep. 72 (1), 1–58. https://doi.org/10.1016/j.surfrep.2017.02.001.
Hendraningrat, L., Li, S.D., Torsæter, O., 2013. A coreflood investigation of nanofluid enhanced oil recovery. J. Petrol. Sci. Eng. 111, 128–138. https://doi.org/10.1016/j.petrol.2013.07.003.
Hendraningrat, L., Torsæter, O., 2015. Metal oxide-based nanoparticles: revealing their potential to enhance oil recovery in different wettability systems. Appl. Nanosci. 5 (2), 181–199. https://doi.org/10.1007/s13204-014-0305-6.
Hill, D., Barron, A.R., Alexander, S., 2020. Controlling the wettability of plastic by thermally embedding coated aluminium oxide nanoparticles into the surface. J. Colloid Interface Sci. 567, 45–53. https://doi.org/10.1016/j.jcis.2020.01.116.
Hirasaki, G.J., 1991. SPE-17367-PA. Wettability: fundamentals and surface forces, 6, pp. 217–226. https://doi.org/10.1103/RevModPhys.57.827, 2.
Hong, L., Jiang, S., Granick, S., 2006. Simple method to produce Janus colloidal particles in large quantity. Langmuir 22 (23), 9495–9499. https://doi.org/10.1021/la062716z.
Hou, B., Jia, R., Wang, Y., et al., 2019. Wettability alteration of oil-wet carbonate surface induced by self-dispersing silica nanoparticles: mechanism and monovalent metal ion's effect. J. Mol. Liq. 294, 111601. https://doi.org/10.1016/j.molliq.2019.111601.
Hu, Z., Azmi, S.M., Raza, G., et al., 2016. Nanoparticle-assisted water-flooding in berea sandstones. Energy Fuel. 30 (4), 2791–2804. https://doi.org/10.1021/acs.energyfuels.6b00051.
Huang, J., Wang, X., Long, Q., et al., 2009. Influence of pH on the Stability Characteristics of Nanofluids. In: 2009 Symposium on Photonics and Optoelectronics, 879–+.
Ismay, M.J.L., Doroodchi, E., Moghtaderi, B., 2013. Effects of colloidal properties on sensible heat transfer in water-based titania nanofluids, 91, pp. 426–436. https://doi.org/10.1016/j.cherd.2012.10.005, 3.
Jang, H.C., Lee, W., Lee, J., 2018. Nanoparticle dispersion with surface-modified silica nanoparticles and its effect on the wettability alteration of carbonate rocks. Colloid. Surface. Physicochem. Eng. Aspect. 554, 261–271. https://doi.org/10.1016/j.colsurfa.2018.06.045.
Ji, X.Y., Zhang, Q., Liang, F.X., et al., 2014. Ionic liquid functionalized Janus nanosheets. Chem. Commun. 50 (43), 5706–5709. https://doi.org/10.1039/c4cc00649f.
Ji, Y., 2014. Ions removal by iron nanoparticles: a study on solid–water interface with zeta potential. Colloid. Surface. Physicochem. Eng. Aspect. 444, 1–8. https://doi.org/10.1016/j.colsurfa.2013.12.031.
Jia, F., Liang, F., Yang, Z., 2016. Janus mesoporous nanodisc from gelable triblock copolymer. ACS Macro Lett. 5 (12), 1344–1347. https://doi.org/10.1021/acsmacrolett.6b00812.
Kamal, M.S., Adewunmi, A.A., Sultan, A.S., et al., 2017. Recent advances in nanoparticles enhanced oil recovery: rheology, interfacial tension, oil recovery, and wettability alteration. J. Nanomater., 2473175 https://doi.org/10.1155/2017/2473175.
Kamiya, H., Iijima, M., 2010. Surface modification and characterization for dispersion stability of inorganic nanometer-scaled particles in liquid media. Sci. Technol. Adv. Mater. 11 (4). https://doi.org/10.1088/1468-6996/11/4/044304, 044304-044304.
Kang, W., Cao, C., Guo, S., et al., 2019. Mechanism of silica nanoparticles' better-thickening effect on amphiphilic polymers in high salinity condition. J. Mol. Liq. 277, 254–260. https://doi.org/10.1016/j.molliq.2018.12.092.
Karambeigi, M.S., Abbassi, R., Roayaei, E., et al., 2015. Emulsion flooding for enhanced oil recovery: interactive optimization of phase behavior, microvisual and core-flood experiments. J. Ind. Eng. Chem. 29, 382–391. https://doi.org/10.1016/j.jiec.2015.04.019.
Karimi, A., Fakhroueian, Z., Bahramian, A., et al., 2012. Wettability alteration in carbonates using zirconium oxide nanofluids: EOR implications. Energy Fuel. 26 (2), 1028–1036. https://doi.org/10.1021/ef201475u.
Kazemzadeh, Y., Sharifi, M., Riazi, M., et al., 2018. Potential effects of metal oxide/SiO_2 nanocomposites in EOR processes at different pressures. Colloid. Surface. Physicochem. Eng. Aspect. 559, 372–384. https://doi.org/10.1016/j.colsurfa.2018.09.068.
Keller, A.A., Wang, H.T., Zhou, D.X., et al., 2010. Stability and aggregation of metal oxide nanoparticles in natural aqueous matrices. Environ. Sci. Technol. 44 (6), 1962–1967. https://doi.org/10.1021/es902987d.
Khalil, M., Jan, B.M., Tong, C.W., et al., 2017. Advanced nanomaterials in oil and gas industry: design, application and challenges. Appl. Energy 191, 287–310. https://doi.org/10.1016/j.apenergy.2017.01.074.
Kim, H.J., Bang, I.C., Onoe, J., 2009. Characteristic stability of bare Au-water nanofluids fabricated by pulsed laser ablation in liquids. Opt Laser. Eng. 47 (5), 532–538. https://doi.org/10.1016/j.optlaseng.2008.10.011.
Klemm, B., Picchioni, F., Raffa, P., et al., 2018. Star-like branched polyacrylamides by RAFT polymerization, Part II: performance evaluation in enhanced oil recovery (EOR). Ind. Eng. Chem. Res. 57 (27), 8835–8844. https://doi.org/10.1021/acs.iecr.7b03368.

Ko, S., Huh, C., 2019. Use of nanoparticles for oil production applications. J. Petrol. Sci. Eng. 172, 97–114. https://doi.org/10.1016/j.petrol.2018.09.051.
Kondiparty, K., Nikolov, A.D., Wasan, D., et al., 2012. Dynamic spreading of nanofluids on solids. Part I: experimental. Langmuir 28 (41), 14618–14623. https://doi.org/10.1021/la3027013.
Konefał, A., Lniak, W., Rostocka, J., et al., 2020. Influence of a shape of gold nanoparticles on the dose enhancement in the wide range of gold mass concentration for high-energy X-ray beams from a medical linac. Rep. Practical Oncol. Radiother. 25 (4), 579–585. https://doi.org/10.1016/j.rpor.2020.05.003.
Koroleva, M., Yurtov, E., 2020. Pickering emulsions stabilized with magnetite, gold, and silica nanoparticles: mathematical modeling and experimental study. Colloid. Surface. Physicochem. Eng. Aspect. 601, 125001. https://doi.org/10.1016/j.colsurfa.2020.125001.
Kubowicz, S., Daillant, J., Dubois, M., et al., 2010. Mixed-monolayer-protected gold nanoparticles for emulsion stabilization. Langmuir 26 (3), 1642–1648. https://doi.org/10.1021/la9025238.
Lattuada, M., Hatton, T.A., 2011. Synthesis, properties and applications of Janus nanoparticles. Nano Today 6 (3), 286–308. https://doi.org/10.1016/j.nantod.2011.04.008.
Lau, H.C., Yu, M., Nguyen, Q.P., 2017. Nanotechnology for oilfield applications: challenges and impact. J. Petrol. Sci. Eng. 157, 1160–1169. https://doi.org/10.1016/j.petrol.2017.07.062.
Lee, J.G., Larive, L.L., Valsaraj, K.T., et al., 2018. Binding of lignin nanoparticles at oil–water interfaces: an ecofriendly alternative to oil spill recovery. Acs Appl. Mater. Interfaces 10 (49), 43282–43289. https://doi.org/10.1021/acsami.8b17748.
Li, C.C., Li, Y., Pu, H., 2021. Molecular simulation study of interfacial tension reduction and oil detachment in nanochannels by Surface-modified silica nanoparticles. Fuel 292, 120318. https://doi.org/10.1016/j.fuel.2021.120318.
Li, J., Li, X., Wu, K., et al., 2017a. Thickness and stability of water film confined inside nanoslits and nanocapillaries of shale and clay. Int. J. Coal Geol. 179, 253–268. https://doi.org/10.1016/j.coal.2017.06.008.
Li, S., Li, Z., Wang, P., 2016. Experimental study of the stabilization of CO_2 foam by sodium dodecyl sulfate and hydrophobic nanoparticles. Ind. Eng. Chem. Res. 55 (5), 1243–1253. https://doi.org/10.1021/acs.iecr.5b04443.
Li, S.Y., Yang, K., Li, Z.M., et al., 2019a. Properties of CO_2 foam stabilized by hydrophilic nanoparticles and nonionic surfactants. Energy Fuel. 33 (6), 5043–5054. https://doi.org/10.1021/acs.energyfuels.9b00773.
Li, X.K., Chen, W.J., Zou, C.J., 2020. The stability, viscosity and thermal conductivity of carbon nanotubes nanofluids with high particle concentration: a surface modification approach. Powder Technol. 361, 957–967. https://doi.org/10.1016/j.powtec.2019.10.106.
Li, X.F., Zhu, D.S., Wang, X.J., 2007. Evaluation on dispersion behavior of the aqueous copper nano-suspensions. J. Colloid Interface Sci. 310 (2), 456–463. https://doi.org/10.1016/j.jcis.2007.02.067.
Li, Y.Y., Dai, C.L., Zhou, H.D., et al., 2017b. A novel nanofluid based on fluorescent carbon nanoparticles for enhanced oil recovery. Ind. Eng. Chem. Res. 56 (44), 12464–12470. https://doi.org/10.1021/acs.iecr.7b03617.
Li, Y.Y., Dai, C.L., Zhou, H.D., et al., 2018a. Investigation of spontaneous imbibition by using a surfactant-free active silica water-based nanofluid for enhanced oil recovery. Energy Fuel. 32 (1), 287–293. https://doi.org/10.1021/acs.energyfuels.7b03132.
Li, Z., Bai, B.J., Xu, D.R., et al., 2019b. Synergistic collaboration between regenerated cellulose and surfactant to stabilize oil/water (O/W) emulsions for enhancing oil recovery. Energy Fuel. 33 (1), 81–88. https://doi.org/10.1021/acs.energyfuels.8b02999.
Li, Z., Wu, H.R., Yang, M., et al., 2018b. Stability mechanism of O/W Pickering emulsions stabilized with regenerated cellulose. Carbohydr. Polym. 181, 224–233. https://doi.org/10.1016/j.carbpol.2017.10.080.
Liang, F.X., Shen, K., Qu, X.Z., et al., 2011. Inorganic Janus nanosheets. Angew. Chem. Int. Ed. 50 (10), 2379–2382. https://doi.org/10.1002/anie.201007519.
Liang, T., Hou, J.R., Qu, M., et al., 2020a. Mechanisms of stabilizing pickering emulsions by two-dimensional smart black nano-card. Oilfield Chem. 37 (2), 297–304. https://doi.org/10.19346/j.cnki.1000-4092.2020.02.020.
Liang, T., Hou, J.R., Qu, M., et al., 2020b. High-viscosity α-starch nanogel particles to enhance oil recovery. RSC Adv. 10 (14), 8275–8285. https://doi.org/10.1039/C9RA06938K.
Liu, J.H., Liu, G.N., Zhang, M.M., et al., 2013. Synthesis and self-assembly of amphiphilic Janus laponite disks. Macromolecules 46 (15), 5974–5984. https://doi.org/10.1021/ma4007363.
Liu, P., Yu, H., Niu, L., et al., 2020. Utilization of Janus-silica/surfactant nanofluid without ultra-low interfacial tension for improving oil recovery. Chem. Eng. Sci. 228, 115964. https://doi.org/10.1016/j.ces.2020.115964.
Liu, Y., Liang, F., Wang, Q., et al., 2015. Flexible responsive Janus nanosheets. Chem. Commun. 51 (17), 3562–3565. https://doi.org/10.1039/c4cc08420a.
Lombardo, D., Kiselev, M.A., Magazù, S., et al., 2015. Amphiphiles self-assembly: basic concepts and future perspectives of supramolecular approaches. Adv. Condens. Matter Phys. 1–22. https://doi.org/10.1155/2015/151683.
Lu, T., Li, Z., Zhou, Y., et al., 2017. Enhanced oil recovery of low-permeability cores by SiO_2 nanofluid. Energy Fuel. 31 (5), 5612–5621. https://doi.org/10.1021/acs.energyfuels.7b00144.
Luo, D., Wang, F., Vu, B.V., et al., 2018. Synthesis of graphene-based amphiphilic Janus nanosheets via manipulation of hydrogen bonding. Carbon 126, 105–110. https://doi.org/10.1016/j.carbon.2017.09.102.
Lv, M., Liu, Y., Geng, J., et al., 2018. Engineering nanomaterials-based biosensors for food safety detection. Biosens. Bioelectron. 106, 122–128. https://doi.org/10.1016/j.bios.2018.01.049.
Ma, H., Luo, M.X., Dai, L.L., 2008. Influences of surfactant and nanoparticle assembly on effective interfacial tensions. Phys. Chem. Chem. Phys. 10 (16), 2207–2213. https://doi.org/10.1039/b718427c.
Ma, X.K., Lee, N.H., Oh, H.J., et al., 2010. Surface modification and characterization of highly dispersed silica nanoparticles by a cationic surfactant. Colloid. Surface. Physicochem. Eng. Aspect. 358 (1), 172–176. https://doi.org/10.1016/j.colsurfa.2010.01.051.
Maghzi, A., Mohammadi, S., Ghazanfari, M.H., et al., 2012. Monitoring wettability alteration by silica nanoparticles during water flooding to heavy oils in five-spot systems: a pore-level investigation. Exp. Therm. Fluid Sci. 40, 168–176. https://doi.org/10.1016/j.expthermflusci.2012.03.004.
Metin, C.O., Baran, J.R., Nguyen, Q.P., 2012. Adsorption of surface functionalized silica nanoparticles onto mineral surfaces and decane/water interface. J. Nanoparticle Res. 14 (11), 1246. https://doi.org/10.1007/s11051-012-1246-1.
Morozovska, A.N., Eliseev, E.A., Fomichov, Y.M., et al., 2020. Electric field control of three-dimensional vortex states in core-shell ferroelectric nanoparticles. Acta Mater. 200, 256–273. https://doi.org/10.2139/ssrn.3581341.
Munshi, A.M., Singh, V.N., Kumar, M., et al., 2008. Effect of nanoparticle size on sessile droplet contact angle. J. Appl. Phys. 103 (8), 084315. https://doi.org/10.1063/1.2912464.
Negin, C., Ali, S., Xie, Q., 2016. Application of nanotechnology for enhancing oil recovery – a review. Petroleum 2 (4), 324–333. https://doi.org/10.1016/j.petlm.2016.10.002.
Negin, C., Ali, S., Xie, Q., 2017. Most common surfactants employed in chemical enhanced oil recovery. Petroleum 3 (2), 197–211. https://doi.org/10.1016/j.petlm.2016.11.007.
Ning, J., Wei, B., Mao, R.X., et al., 2018. Pore-level observations of an alkali-induced mild O/W emulsion flooding for economic enhanced oil recovery. Energy Fuel. 32 (10), 10595–10604. https://doi.org/10.1021/acs.energyfuels.8b02493.
Nowrouzi, I., Manshad, A.K., Mohammadi, A.H., 2019. Effects of TiO_2, MgO, and γ-Al_2O_3 nano-particles in carbonated water on water-oil interfacial tension (IFT) reduction in chemical enhanced oil recovery (CEOR) process. J. Mol. Liq. 292, 111348. https://doi.org/10.1016/j.molliq.2019.111348.
Omran, M., Akarri, S., Torsaeter, O., 2020. The effect of wettability and flow rate on oil displacement using polymer-coated silica nanoparticles: a microfluidic study. Processes 8 (8). https://doi.org/10.3390/pr8080991.
Parvazdavani, M., Masihi, M., Ghazanfari, M.H., 2014. Monitoring the influence of dispersed nano-particles on oil–water relative permeability hysteresis. J. Petrol. Sci. Eng. 124, 222–231. https://doi.org/10.1016/j.petrol.2014.10.005.
Pate, K., Safier, P., 2016. 12 - chemical metrology methods for CMP quality. In: Babu, S. (Ed.), Advances in Chemical Mechanical Planarization (CMP). Woodhead Publishing, pp. 299–325. https://doi.org/10.1016/B978-0-08-100165-3.00012-7.
Patel, H., Shah, S., Ahmed, R., et al., 2018. Effects of nanoparticles and temperature on heavy oil viscosity. J. Petrol. Sci. Eng. 167, 819–828. https://doi.org/10.1016/j.petrol.2018.04.069.
Pichot, R., Spyropoulos, F., Norton, I.T., 2012. Competitive adsorption of surfactants and hydrophilic silica particles at the oil–water interface: interfacial tension and contact angle studies. J. Colloid Interface Sci. 377 (1), 396–405. https://doi.org/10.1016/j.jcis.2012.01.065.
Qu, M., Hou, J.R., Liang, T., et al., 2021. Amphiphilic rhamnolipid molybdenum disulfide nanosheets for oil recovery. ACS Appl. Nano Mater. https://doi.org/10.1021/acsanm.1c00102.
Qu, M., Hou, J.R., Liang, T., et al., 2020. Preparation and interfacial properties of ultralow concentrations of amphiphilic molybdenum disulfide nanosheets. Ind. Eng. Chem. Res. 59 (19), 9066–9075. https://doi.org/10.1021/acs.iecr.0c00217.
Raj, I., Qu, M., Xiao, L., et al., 2019. Ultralow concentration of molybdenum disulfide nanosheets for enhanced oil recovery. Fuel 251, 514–522. https://doi.org/10.1016/j.fuel.2019.04.078.
Rattanaudom, P., Shiau, B.J., Suriyapraphadilok, U., et al., 2021. Effect of pH on silica nanoparticle-stabilized foam for enhanced oil recovery using carboxylate-based extended surfactants. J. Petrol. Sci. Eng. 196, 107729. https://doi.org/10.1016/j.petrol.2020.107729.
Ravera, F., Santini, E., Loglio, G., et al., 2006. Effect of nanoparticles on the interfacial properties of liquid/liquid and liquid/air surface layers. J. Phys. Chem. B 110 (39), 19543–19551. https://doi.org/10.1021/jp0636468.
Rezk, M.Y., Allam, N.K., 2019. Impact of nanotechnology on enhanced oil recovery: a mini-review. Ind. Eng. Chem. Res. 58 (36), 16287–16295. https://doi.org/10.1021/acs.iecr.9b03693.
Rezvani, H., Panahpoori, D., Riazi, M., et al., 2020. A novel foam formulation by Al_2O_3/SiO_2 nanoparticles for EOR applications: a mechanistic study. J. Mol. Liq. 304, 112730. https://doi.org/10.1016/j.molliq.2020.112730.
Rosen, M.J., Wang, H.Z., Shen, P.P., et al., 2005. Ultralow interfacial tension for enhanced oil recovery at very low surfactant concentrations. Langmuir 21 (9), 3749–3756. https://doi.org/10.1021/la0400959.
Roustaei, A., Saffarzadeh, S., Mohammadi, M., 2013. An evaluation of modified silica nanoparticles' efficiency in enhancing oil recovery of light and intermediate oil reservoirs. Egypt. J. Petrol. 22 (3), 427–433. https://doi.org/10.1016/j.ejpe.2013.06.010.
Saleh, N., Kim, H.J., Phenrat, T., et al., 2008. Ionic strength and composition affect the mobility of surface-modified FeO nanoparticles in water-saturated sand columns. Environ. Sci. Technol. 42 (9), 3349–3355. https://doi.org/10.1021/es071936b.

Seetharaman, G.R., Jadhav, R.M., Sangwai, J.S., 2020. Effect of monovalent and divalent alkali [(NaOH and $Ca(OH)_2$] on the interfacial tension of pure hydrocarbon-water systems relevant for enhanced oil recovery. J. Petrol. Sci. Eng., 107892 https://doi.org/10.1016/j.petrol.2020.107892.
Shah, A., Fishwick, R., Wood, J., et al., 2010. A review of novel techniques for heavy oil and bitumen extraction and upgrading. Energy Environ. Sci. 3 (6), 700–714. https://doi.org/10.1039/b918960b.
Shaker, S.B., Skauge, A., 2013. Enhanced oil recovery (EOR) by combined low salinity water/polymer flooding. Energy Fuel. 27 (3), 1223–1235. https://doi.org/10.1021/ef301538e.
Shalbafan, M., Esmaeilzadeh, F., Safaei, A., et al., 2019. Experimental investigation of wettability alteration and oil recovery enhance in carbonate reservoirs using iron oxide nanoparticles coated with EDTA or SLS. J. Petrol. Sci. Eng. 180, 559–568. https://doi.org/10.1016/j.petrol.2019.05.085.
Shamsi, J.H., Miller, C.A., Wong, M.S., et al., 2014. Polymer-coated nanoparticles for enhanced oil recovery. J. Appl. Polym. Sci. 131 (15). https://doi.org/10.1002/app.40576.
Sikiru, S., Rostami, A., Soleimani, H., et al., 2021. Graphene: outlook in the enhance oil recovery (EOR). J. Mol. Liq. 321, 114519. https://doi.org/10.1016/j.molliq.2020.114519.
Singh, Y., Singh, N.K., Sharma, A., et al., 2021. Effect of ZnO nanoparticles concentration as additives to the epoxidized Euphorbia Lathyris oil and their tribological characterization. Fuel 285, 119148. https://doi.org/10.1016/j.fuel.2020.119148.
Sofla, S.J.D., James, L.A., Zhang, Y.H., 2018. Insight into the stability of hydrophilic silica nanoparticles in seawater for Enhanced oil recovery implications. Fuel 216, 559–571. https://doi.org/10.1016/j.fuel.2017.11.091.
Sohel, M.S.M., Tan, S.H., Nguyen, N.T., 2008. Temperature dependence of interfacial properties and viscosity of nanofluids for droplet-based microfluidics. J. Phys. Appl. Phys. 41 (8), 085502. https://doi.org/10.1088/0022-3727/41/8/085502.
Souza, N.S., Rodrigues, A.D., Cardoso, C.A., et al., 2012. Physical properties of nanofluid suspension of ferromagnetic graphite with high Zeta potential. Phys. Lett. 376 (4), 544–546. https://doi.org/10.1016/j.physleta.2011.11.050.
Stancik, E.J., Kouhkan, M., Fuller, G.G., 2004. Coalescence of particle-laden fluid interfaces. Langmuir 20 (1), 90–94. https://doi.org/10.1021/la0356093.
Sun, Q., Li, Z.M., Wang, J.Q., et al., 2015. Aqueous foam stabilized by partially hydrophobic nanoparticles in the presence of surfactant. Colloid. Surface. Physicochem. Eng. Aspect. 471, 54–64. https://doi.org/10.1016/j.colsurfa.2015.02.007.
Sun, Y.X., Yang, D.H., Shi, L.C., et al., 2020. Properties of nanofluids and their applications in enhanced oil recovery: a comprehensive review. Energy Fuel. 34 (2), 1202–1218. https://doi.org/10.1021/acs.energyfuels.9b03501.
Taborda, E.A., Franco, C.A., Lopera, S.H., et al., 2021. Effect of surface acidity of SiO_2 nanoparticles on thermal stability of polymer solutions for application in EOR processes. J. Petrol. Sci. Eng. 196, 107802. https://doi.org/10.1016/j.petrol.2020.107802.
Tackie-otoo, B.N., Ayoub, M.M.A., 2020. Experimental investigation of the behaviour of a novel amino acid-based surfactant relevant to EOR application. J. Mol. Liq. 316, 113848. https://doi.org/10.1016/j.molliq.2020.113848.
Tambe, D.E., Sharma, M.M., 1995. Factors controlling the stability of colloid-stabilized emulsions: III. Measurement of the rheological properties of colloid-laden interfaces. J. Colloid Interface Sci. 171 (2), 456–462. https://doi.org/10.1006/jcis.1995.1202.
Tod, V., Rsd, M., Pfd, A., et al., 2020. The impact of alkyl polyglycoside surfactant on oil yields and its potential effect on the biogenic souring during enhanced oil recovery (EOR). Fuel 280, 118512. https://doi.org/10.1016/j.fuel.2020.118512.
Trokhymchuk, A., Henderson, D., Nikolov, A., et al., 2001. A simple calculation of structural and depletion forces for fluids/suspensions confined in a film. Langmuir 17 (16), 4940–4947. https://doi.org/10.1021/la010047d.
Tyowua, A.T., Yiase, S.G., Binks, B.P., 2017. Double oil-in-oil-in-oil emulsions stabilised solely by particles. J. Colloid Interface Sci. 488, 127–134. https://doi.org/10.1016/j.jcis.2016.10.089.
Walther, A., Hoffmann, M., Muller, A.H.E., 2008. Emulsion polymerization using Janus particles as stabilizers. Angew. Chem. Int. Ed. 47 (4), 711–714. https://doi.org/10.1002/anie.200703224.
Wan, Z.T., Li, D., Jiao, Y.L., et al., 2017. Bifunctional MoS_2 coated melamine-formaldehyde sponges for efficient oil–water separation and water-soluble dye removal. Appl. Mater. Today 9, 551–559. https://doi.org/10.1016/j.apmt.2017.09.013.
Wan, Z.T., Liu, Y.C.Y., Chen, S.D., et al., 2018. Facile fabrication of a highly durable and flexible MoS_2@RTV sponge for efficient oil-water separation. Colloid. Surface. Physicochem. Eng. Aspect. 546, 237–243. https://doi.org/10.1016/j.colsurfa.2018.03.017.
Wang, T., Zhang, Y., Li, L., et al., 2018. Experimental study on pressure-decreasing performance and mechanism of nanoparticles in low permeability reservoir. J. Petrol. Sci. Eng. 166, 693–703. https://doi.org/10.1016/j.petrol.2018.03.070.
Wasan, D.T., Nikolov, A.D., 2003. Spreading of nanofluids on solids. Nature 423 (6936), 156–159. https://doi.org/10.1038/nature01591.
Wei, B., Li, H., Li, Q.Z., et al., 2018. Investigation of synergism between surface-grafted nano-cellulose and surfactants in stabilized foam injection process. Fuel 211, 223–232. https://doi.org/10.1016/j.fuel.2017.09.054.
Wu, H., Gao, K., Lu, Y., et al., 2020. Silica-based amphiphilic Janus nanofluid with improved interfacial properties for enhanced oil recovery. Colloid. Surface. Physicochem. Eng. Aspect. 586, 124162. https://doi.org/10.1016/j.colsurfa.2019.124162.
Wu, H., Yi, W.Y., Chen, Z., et al., 2015. Janus graphene oxide nanosheets prepared via Pickering emulsion template. Carbon 93, 473–483. https://doi.org/10.1016/j.carbon.2015.05.083.
Xiong, K., Zhou, L.Y., Wang, J.Y., et al., 2020. Construction of food-grade pH-sensitive nanoparticles for delivering functional food ingredients. Trends Food Sci. Technol. 96, 102–113. https://doi.org/10.1016/j.tifs.2019.12.019.
Xu, Z.X., Li, B.F., Zhao, H.Y., et al., 2020. Investigation of the effect of nanoparticle-stabilized foam on EOR: nitrogen foam and methane foam. ACS Omega 5 (30), 19092–19103. https://doi.org/10.1021/acsomega.0c02434.
Yakasai, F., Jaafar, M.Z., Bandyopadhyay, S., et al., 2021. Current developments and future outlook in nanofluid flooding: a comprehensive review of various parameters influencing oil recovery mechanisms. J. Ind. Eng. Chem. 93, 138–162. https://doi.org/10.1016/j.jiec.2020.10.017.
Yan, J., Chaudhary, K., Bae, S.C., et al., 2013. Colloidal ribbons and rings from Janus magnetic rods. Nat. Commun. 4. https://doi.org/10.1038/ncomms2520.
Yang, H., Su, Z., Meng, X., et al., 2020. Fabrication and characterization of Pickering emulsion stabilized by soy protein isolate-chitosan nanoparticles. Carbohydr. Polym. 247. https://doi.org/10.1016/j.carbpol.2020.116712.
Yang, K., Li, S., Zhang, K., et al., 2021. Synergy of hydrophilic nanoparticle and nonionic surfactant on stabilization of carbon dioxide-in-brine foams at elevated temperatures and extreme salinities. Fuel 288, 119624. https://doi.org/10.1016/j.fuel.2020.119624.
Yang, W., Wang, T., Fan, Z., 2017. Highly stable foam stabilized by alumina nanoparticles for EOR: effects of sodium cumenesulfonate and electrolyte concentrations. Energy Fuel. 31 (9), 9016–9025. https://doi.org/10.1021/acs.energyfuels.7b01248.
Yang, Y., Lei, Z., Zhang, L., et al., 2016. Preparation of Janus Graphene Oxide (GO) Nanosheets Based on Electrostatic Assembly of GO Nanosheets and Polystyrene Microspheres, 37, pp. 1520–1526. https://doi.org/10.1002/marc.201600308, 18.
Yin, X., Kang, W., Song, S., et al., 2018. Stabilization mechanism of CO_2 foam reinforced by regenerated cellulose. Colloid. Surface. Physicochem. Eng. Aspect. 555, 754–764. https://doi.org/10.1016/j.colsurfa.2018.07.042.
Yoon, K.Y., Li, Z., Neilson, B.M., et al., 2012. Effect of adsorbed amphiphilic copolymers on the interfacial activity of superparamagnetic nanoclusters and the emulsification of oil in water. Macromolecules 45 (12), 5157–5166. https://doi.org/10.1021/ma202511b.
Yu, H.W., Hui, G., Kang, J.X., et al., 2020. Applicability of a nano-silica microemulsion for depressureization and injection of low permeability reservoirs. Drill. Prod. Technol. 43 (2), 111–114+7. https://doi.org/10.3969/J.ISSN.1006-768X.2020.02.30.
Zaid, H.M., Yahya, N., Latiff, N.R.A., 2013. The effect of nanoparticles crystallite size on the recovery efficiency in dielectric nanofluid flooding. J. Nano Res. 21, 103–108. https://doi.org/10.4028/www.scientific.net/JNanoR.21.103.
Zhang, H., Nikolov, A., Wasan, D., 2014. Dewetting film dynamics inside a capillary using a micellar nanofluid. Langmuir 30 (31), 9430–9435. https://doi.org/10.1021/la502387j.
Zhang, H., Ramakrishnan, T.S., Nikolov, A., et al., 2016. Enhanced oil recovery driven by nanofilm structural disjoining pressure: flooding experiments and microvisualization. Energy Fuel. 30 (4), 2771–2779. https://doi.org/10.1021/acs.energyfuels.6b00035.
Zhang, L., Yu, J., Yang, M., et al., 2013. Janus graphene from asymmetric two-dimensional chemistry. Nat. Commun. 4 (1), 1443. https://doi.org/10.1038/ncomms2464.
Zhang, Y., Zhou, F., Zhao, M., et al., 2018. Soy peptide nanoparticles by ultrasound-induced self-assembly of large peptide aggregates and their role on emulsion stability. Food Hydrocolloids 74, 62–71. https://doi.org/10.1016/j.foodhyd.2017.07.021.
Zhao, J., Wen, D.S., 2017. Pore-scale simulation of wettability and interfacial tension effects on flooding process for enhanced oil recovery. RSC Adv. 7 (66), 41391–41398. https://doi.org/10.1039/c7ra07325a.
Zhou, H.T., Liang, Y.P., Huang, P., et al., 2018. Systematic investigation of ionic liquid-type gemini surfactants and their abnormal salt effects on the interfacial tension of a water/model oil system. J. Mol. Liq. 249, 33–39. https://doi.org/10.1016/j.molliq.2017.11.004.
Zhou, K., Zhou, X., Liu, J., et al., 2020. Application of magnetic nanoparticles in petroleum industry: a review. J. Petrol. Sci. Eng. 188, 106943. https://doi.org/10.1016/j.petrol.2020.106943.
Zhou, Y.X., Zhong, X., Sun, W., et al., 2019. Surfactant-augmented functional silica nanoparticle based nanofluid for enhanced oil recovery at high temperature and salinity. Acs Appl. Mater. Interfaces 11 (49), 45763–45775. https://doi.org/10.1021/acsami.9b16960.
Zhu, D.S., Li, X.F., Wang, N., et al., 2009. Dispersion behavior and thermal conductivity characteristics of Al_2O_3–H_2O nanofluids. Curr. Appl. Phys. 9 (1), 131–139. https://doi.org/10.1016/j.cap.2007.12.008.